



# **NAVAL POSTGRADUATE SCHOOL**

**MONTEREY, CALIFORNIA**

## **THESIS**

**MODELING OF LOW TEMPERATURE C-V PROFILING IN  
BLOCKED IMPURITY BAND DETECTORS**

by

Steven J. Tschanz

September 2005

Thesis Advisor:  
Co-Advisor:

Nancy M. Haegel  
Donald L. Walters

**Approved for public release; distribution is unlimited**

THIS PAGE INTENTIONALLY LEFT BLANK

<b>REPORT DOCUMENTATION PAGE</b>			<i>Form Approved OMB No. 0704-0188</i>	
Public reporting burden for this collection of information is estimated to average 1 hour per response, including the time for reviewing instruction, searching existing data sources, gathering and maintaining the data needed, and completing and reviewing the collection of information. Send comments regarding this burden estimate or any other aspect of this collection of information, including suggestions for reducing this burden, to Washington headquarters Services, Directorate for Information Operations and Reports, 1215 Jefferson Davis Highway, Suite 1204, Arlington, VA 22202-4302, and to the Office of Management and Budget, Paperwork Reduction Project (0704-0188) Washington DC 20503.				
<b>1. AGENCY USE ONLY (Leave blank)</b>		<b>2. REPORT DATE</b> September 2005	<b>3. REPORT TYPE AND DATES COVERED</b> Master's Thesis	
<b>4. TITLE AND SUBTITLE:</b> Modeling Low Temperature C-V Profiling in Blocked Impurity Band Detectors			<b>5. FUNDING NUMBERS</b>	
<b>6. AUTHOR(S)</b> Steve J. Tschanz				
<b>7. PERFORMING ORGANIZATION NAME(S) AND ADDRESS(ES)</b> Naval Postgraduate School Monterey, CA 93943-5000			<b>8. PERFORMING ORGANIZATION REPORT NUMBER</b>	
<b>9. SPONSORING /MONITORING AGENCY NAME(S) AND ADDRESS(ES)</b> NASA Ames Research Laboratory, Moffett Field CA.			<b>10. SPONSORING/MONITORING AGENCY REPORT NUMBER</b>	
<b>11. SUPPLEMENTARY NOTES</b> The views expressed in this thesis are those of the author and do not reflect the official policy or position of the Department of Defense or the U.S. Government.				
<b>12a. DISTRIBUTION / AVAILABILITY STATEMENT</b> Approved for public release; distribution is unlimited			<b>12b. DISTRIBUTION CODE</b>	
<b>13. ABSTRACT (maximum 200 words)</b> Silicon Blocked Impurity Band (BIB) detectors are state-of-the-art devices to detect light in the near to mid infrared range (5-40 $\mu$ m). Numerical modeling of BIB detectors is performed using a four-region finite difference approach to study the role of space charge in C-V (capacitance-voltage) profiling of minority carrier doping and the role of blocking layer thickness and minority doping concentration in alternate bias operation. Compensation in the blocking layer is found to play a critical role in determining the net voltage drop in this part of the device under alternate polarity bias. The effect of space charge at the blocking layer/active layer interface on the measured low temperature C-V distribution is modeled as a function of the doping interface between the two layers. The magnitude of the space charge can cause large deviations in the measurement of minority doping concentration from the idealized case which assumes a space-charge free blocking layer and interface. Accurately determining these minority doping concentrations is a crucial step toward solving material growth challenges in proposed far infrared Ge and GaAs devices.				
<b>14. SUBJECT TERMS</b> Blocked Impurity Band (BIB), Impurity Band Conduction (IBC), Infrared Detector, Infrared Sensors, Long Wavelength Infrared (LWIR), Very Long Wavelength Infrared (VLWIR), C-V Profiling, Low Temperature C-V Profiling, Minority Doping Concentration			<b>15. NUMBER OF PAGES</b> 67	
			<b>16. PRICE CODE</b>	
<b>17. SECURITY CLASSIFICATION OF REPORT</b> Unclassified	<b>18. SECURITY CLASSIFICATION OF THIS PAGE</b> Unclassified	<b>19. SECURITY CLASSIFICATION OF ABSTRACT</b> Unclassified	<b>20. LIMITATION OF ABSTRACT</b> UL	

NSN 7540-01-280-5500

Standard Form 298 (Rev. 2-89)  
Prescribed by ANSI Std. Z39-18

THIS PAGE INTENTIONALLY LEFT BLANK

**Approved for public release; distribution is unlimited**

**MODELING LOW TEMPERATURE C-V PROFILING IN BLOCKED IMPURITY  
BAND DETECTORS**

Steven J. Tschanz  
Ensign, United States Naval Reserves  
B. S., University of Notre Dame, 2004

Submitted in partial fulfillment of the  
requirements for the degree of

**MASTER OF SCIENCE IN APPLIED PHYSICS**

from the

**NAVAL POSTGRADUATE SCHOOL  
September 2005**

Author: Steven J. Tschanz

Approved by: Nancy M. Haegel  
Thesis Advisor

Donald L. Walters  
Co-Advisor

James H. Luscombe  
Chairman, Department of Physics

THIS PAGE INTENTIONALLY LEFT BLANK

## **ABSTRACT**

Silicon Blocked Impurity Band (BIB) detectors are state-of-the-art devices to detect light in the near to mid infrared range (5-40  $\mu$  m). Numerical modeling of BIB detectors is performed using a four-region finite difference approach to study the role of space charge in C-V (capacitance-voltage) profiling of minority carrier doping and the role of blocking layer thickness and minority doping concentration in an alternative bias scheme. Compensation in the blocking layer is found to play a critical role in determining the net voltage drop in this part of the device under alternate polarity bias. The effect of space charge at the blocking layer/active layer interface on the measured low temperature C-V distribution is modeled as a function of the doping interface between the two layers. The magnitude of the space charge can cause large deviations in the measurement of minority doping concentration from the idealized case which assumes a space-charge free blocking layer and interface. Accurately determining these minority doping concentrations is a crucial step toward solving material growth challenges in proposed far infrared Ge and GaAs devices.

THIS PAGE INTENTIONALLY LEFT BLANK



## TABLE OF CONTENTS

I.	INTRODUCTION.....	1
A.	BLOCKED IMPURITY BAND (BIB) DETECTORS.....	1
B.	MILITARY RELEVANCE .....	3
C.	BIB OPERATION .....	4
II.	EXPERIMENTAL SETUP .....	7
A.	COMPUTATION SETUP .....	7
B.	FINITE DIFFERENCE COMPUTER MODEL.....	7
III.	C-V PROFILING METHOD .....	15
A.	GROWTH CONSTRAINTS .....	15
B.	C-V PROFILING METHOD THEORY .....	17
IV.	MODELING RESULTS .....	21
A.	LOW TEMPERATURE C-V MODELING .....	21
B.	INTRODUCING INTERFACE GRADES .....	25
C.	REALISTIC DEVICE PARAMETERS WITH GRADE .....	28
D.	ANALYSIS .....	30
V.	COMPENSATION IN ALTERNATE BIAS .....	37
A.	ALTERNATE BIAS OPERATION .....	37
B.	ALTERNATE CONFIGURATION IN GERMANIUM.....	42
VI.	CONCLUSIONS.....	47
A.	SUMMARY.....	47
B.	FUTURE WORK.....	48
	LIST OF REFERENCES.....	49
	INITIAL DISTRIBUTION LIST .....	51

THIS PAGE INTENTIONALLY LEFT BLANK

## LIST OF FIGURES

Figure 1	BIB wavelength extension. ....	2
Figure 2	Schematic diagram of a standard biased n-type BIB. Red line indicates the electric field distribution. ....	5
Figure 3	Schematic diagram of standard biased p-type BIB. Red line indicates the electric field distribution. ....	6
Figure 4	Plot of doping profile as a function of position for four values of grade parameter ( $g$ from equation 2.16).....	10
Figure 5	BIB input file .....	11
Figure 6	BIB output file .....	12
Figure 7	Active layer compensation effects in GaAs (solid line 0.1%, dashed line 10% compensation) .....	15
Figure 8	Electric field profiles for varied blocking layer thicknesses (10 and 20 $\mu\text{m}$ ) and minority doping levels in a Ge BIB. ....	17
Figure 9	Space charge profile for a Si BIB with a 0.05 V Bias (Table 1).....	21
Figure 10	Modulated change in space charge (left axis, solid) and electric field (right axis, dashed) as a function of position for a case with an ideally sharp interface.....	22
Figure 11	$1/C^2$ and minority doping as a function of applied bias. Parameters listed in Table 1. ....	24
Figure 12	Space charge variations that include near contact space charge (far right). Parameters listed in Table 1.....	25
Figure 13	Low temperature C-V profiling results (Courtesy of P. Love).....	26
Figure 14	Spreading resistance measurement showing graded region, blocking layer starting from the left, active layer $\sim 5 - 35 \mu\text{m}$ (Courtesy of P. Love).....	27
Figure 15	Minority doping concentration as a function of bias for $g=2 \times 10^{-5} \text{ cm}$ . Inset depicts the actual position of space charge, and therefore the minority doping sample area, for several biases. ....	28
Figure 16	$1/C^2$ as a function of applied bias. Parameters listed in Table 1 with varied interface grade.....	29
Figure 17	Compensation calculations from C-V profiling, calculated from Figure 16, as a function of the applied bias. Parameters listed in Table 1 for varied interface grade.....	29
Figure 18	Change in space charge as a function of bias for grade $g=4 \times 10^{-5} \text{ cm}$ .....	31
Figure 19	Grade effects on initial (0.05 V) calculated minority doping.....	33
Figure 20	Expanded field profiles near the interface at 0.05 V bias, varied grade parameters. ....	34
Figure 21	Change in space charge in the blocking layer, grade $g=4 \times 10^{-5} \text{ cm}$ . ...	35
Figure 22	Electric field as a function of position for several blocking layer thicknesses. Parameters the same as Table 1 except active layer minority doping $5 \times 10^{12} \text{ cm}^{-3}$ , temperature 4.2 K, bias 0.75 V. ....	37

Figure 23	Schematic diagram of alternate biased n-type BIB. Red line indicates the electric field distribution. ....	38
Figure 24	Schematic diagram of alternate biased p-type BIB. Red line indicates the electric field distribution. ....	39
Figure 25	Electric field as a function of position for standard and alternate biases. Parameters same as Table 1. ....	40
Figure 26	Hopping current as a function of position for multiple biases and configurations. Parameters the same as Table 1 except active layer minority doping $5 \times 10^{12} \text{ cm}^{-3}$ , temperature 4.2 K.....	41
Figure 27	Plot of free carrier concentration, showing Debye tails for standard and alternate bias. Parameters the same as Table 1 except active layer minority doping $5 \times 10^{12} \text{ cm}^{-3}$ , temperature 4.2 K, bias 0.5 V.....	42
Figure 28	Electric field as a function of position for standard and alternate bias in Ge. Parameters listed in Table 2.....	44
Figure 29	Electric Field as a function of doping, Ge. Parameters listed in Table 2, varied minority doping, alternate biased 0.2 V.....	45

## LIST OF TABLES

Table 1	Si BIB parameters used for C-V simulations .....	23
Table 2	Ge BIB parameters.....	43

THIS PAGE INTENTIONALLY LEFT BLANK

## **ACKNOWLEDGMENTS**

Most importantly I would like to thank my thesis advisor, Professor Nancy Haegel, for a year of continuous patience and encouragement. She made my learning experience at the Naval Postgraduate School extraordinary, and I am indebted to her.

I would also like to thank my fellow lab-mates LCDR Jonathan Garcia, LCDR Mitch Bradley, and Capt David Luber, who set the expectations high from the beginning and never let up. I consider myself lucky to have been able to work with each of them.

I would like to thank colleagues at both NASA Ames and Raytheon Vision Systems, especially Peter Love, for helpful discussions and support throughout.

Finally, I want to thank my fiancée for her support as I spent the year several time zones away. I could not have done this without her.

THIS PAGE INTENTIONALLY LEFT BLANK



## I. INTRODUCTION

### A. BLOCKED IMPURITY BAND (BIB) DETECTORS

Blocked Impurity Band (BIB) detectors, also known as Impurity Band Conduction (IBC) detectors, are highly efficient, radiation hardened extrinsic photodetectors currently used to detect light in the 5-40  $\mu\text{m}$  range. They were first developed in 1986 by Petroff and Stapelbroek at the Rockwell International Science Center [1].

BIB detectors consist of two layers fabricated through liquid or vapor phase epitaxy. One region, the active layer, is heavily doped and is responsible for photon absorption through donor (or acceptor) ionization. This high doping level allows for greater efficiency and reduced volume and is responsible for BIB replacement of standard photoconductors in many applications. The second region is a highly pure layer called the blocking layer. This region limits the current to carriers excited to the conduction (or valence) band of the device.

The small energies used for detection vary with the material and dopant used. For an As doped Si device, the ionization energy is 54 meV. This translates into a cutoff wavelength of about 26  $\mu\text{m}$  and requires an operating temperature of 4-10 K. This wavelength response has been extended with Si:Sb BIBs which have ionization energies of 43 meV and wavelength extension out to 37  $\mu\text{m}$  [2].

Current work is focusing on extending BIB response into the far-infrared range using Ge:Ga and GaAs. Ge:Ga has ionization energies of 10 – 11 meV with wavelength cutoff response to 100  $\mu\text{m}$ , while uniaxial compression can lower these ionization energies and extend response out to 200  $\mu\text{m}$ . GaAs doped with Si or Te demonstrates ground state ionization energies of 5.7 meV with the first excited state transition at an energy of 4.3 meV. These energies represent wavelength response at 217 and 286  $\mu\text{m}$  respectively.

Due to the small energies involved in detecting light in the infrared and especially far-infrared range, the device must be cooled to prevent donor/acceptor sites from becoming ionized producing excessive thermal-excitation into the conduction/valence band. Examples of the various materials and wavelength responses described can be seen in Figure 1. The longer wavelength response materials offer great potential, however fabrication issues continue to hinder the realization of these devices [3].

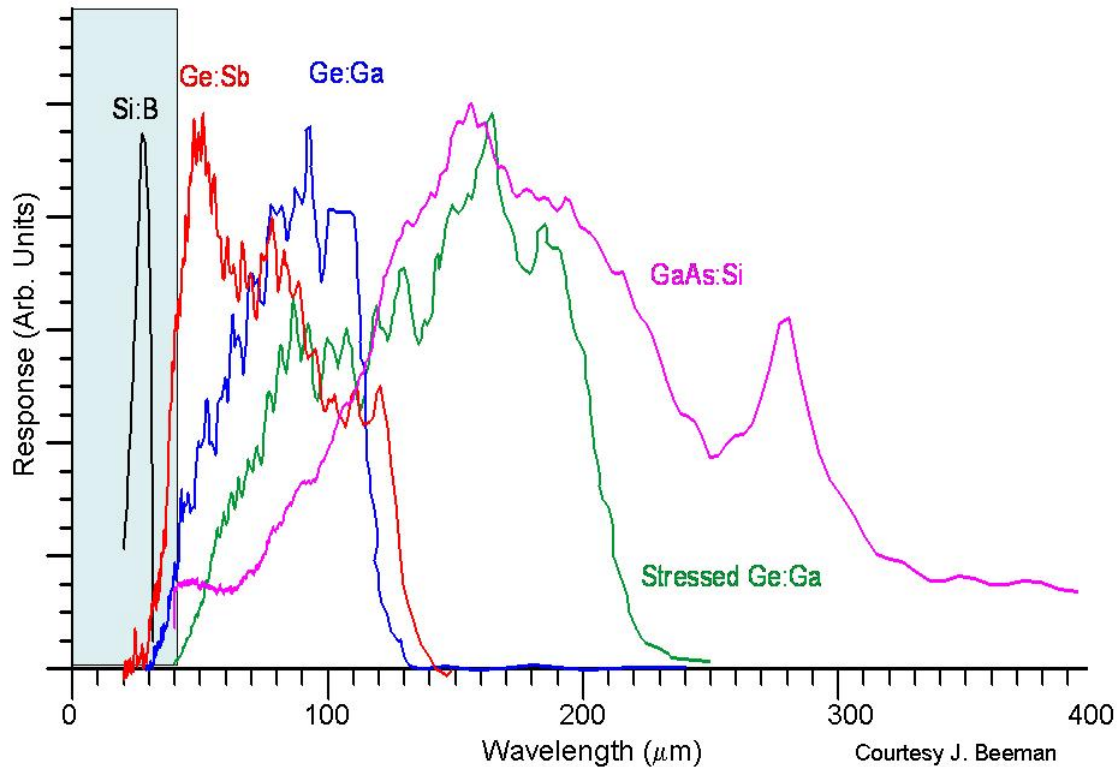


**Figure 1 BIB wavelength extension.**

Foremost among these challenges is growing the extremely thin, highly pure blocking layer the devices require. It can be difficult to grow blocking layers to the purity levels desired. First, the majority doping level ideally must be very low ( $\sim 10^{11} \text{ cm}^{-3}$ ). In addition, the minority doping must be even lower relative to the majority doping level. The compensation of a device region, defined as

$$k = \frac{N_{\text{minority}}}{N_{\text{majority}}} \quad (1.1)$$

must be controlled precisely and kept very low for many applications. Even when these purity levels are attainable, the layer also needs to be grown very thin, and often the blocking layer never attains the ideal doping level. In these cases the blocking layer is simply a transition area from the heavily doped active layer. Diffusion of dopants from the active layer into the blocking layer adds to this graded region. The end result of these combined factors is a transition area with enough doping to allow significant dark current.

The difficulty of these growth challenges leads naturally to application of various methods of device characterization. Inability to directly measure doping characteristics only makes growth challenges more difficult to solve, and investigation and analysis of one of these key techniques, low temperature C-V profiling for minority doping concentrations, will be analyzed in detail.

## **B. MILITARY RELEVANCE**

BIBs were originally intended to provide epitaxial style detectors for the mid-IR range to replace conventional bulk Si photoconductors, which were highly sensitive to degenerative radiation effects. The primary motivation was for defense applications, specifically for ballistic missile defense. The IR response of these detectors makes them ideal for cold body detection and tracking, an important feature for re-entry and late-stage interception and destruction of a missile [4]. In addition a great deal of spectroscopy information is available in this range, so chemical identification using these devices is of significant interest. The highly touted tera-hertz frequencies also lie within this range, which has potential for significantly outperforming x-ray and metal detector devices in security fields. In this area, infrared spectroscopy is of interest to identify chemical species in closed containers. However, these highly sensitive detector arrays have always found a niche in space-based mid-IR astronomy. Used for deep space imaging and spectroscopy, Si:As and Si:Sb BIB devices are currently on the Spitzer Space Telescope and a Si:As BIB array is planned for the James Webb Space Telescope to be launched in 2011 [2,5].

### C. BIB OPERATION

A complete description of BIB operation is difficult because many different doping schemes and bias configurations exist. Several principles are, however, common to all BIB detectors. The operation of the BIB, regardless of type, can be tied to two key characteristics: the use of a heavily doped active layer for collection of light and a pure blocking layer which prevents flow of the hopping current along the dopant band. All BIBs operate by establishing a depletion region in the active layer which collects light through ionization of dopant sites. Once excited to the conduction band (or in the case of holes to the valence band), these carriers create a photocurrent.

In standard bias configuration, a bias is applied to the blocking layer contact, thus depleting through the highly pure blocking layer into the active layer where the necessary depletion region is established. The simplest starting point is shown in Figure 2 with an n-type BIB such as Silicon doped Antimony (Si:Sb), in which the majority dopant has an extra electron, and thus constitutes a donor site. All of the minority acceptor sites in the active layer are ionized by the majority dopants. In this schematic the electric field in the device is represented with a red line. A positive bias is applied to the blocking layer contact, which depletes into the active layer.

Due to the low temperature of operation the electrons remain thermally within the donor band, but are free to move along it in the active layer. Electrons will move to occupy the ionized donors, leaving a net space charge of ionized minority dopants ( $N_A^-$ ). The depletion width is therefore determined by the concentration of minority dopants. In the case of an n-type device this means a positive bias must be applied in order to terminate the electric field lines at the negative ionized acceptors ( $N_A^-$ ). When light ionizes a donor site in the depletion width, the bias moves free electrons toward the blocking layer contact and drives ionized donor ( $N_D^+$ ) sites, the hopping current, toward the active layer contact. Thus, the photocurrent is collected in a standard biased n-type BIB.

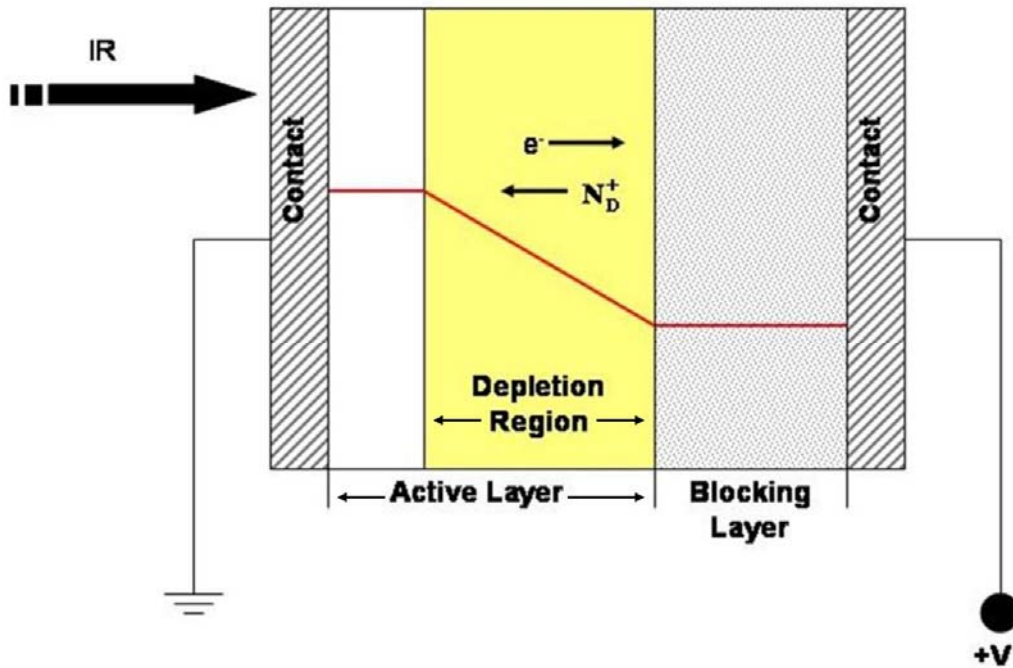


**Figure 2 Schematic diagram of a standard biased n-type BIB. Red line indicates the electric field distribution.**

P-type BIBs such as gallium doped germanium (Ge:Ga) in standard bias configuration, Figure 3, operate similarly only the majority dopants are acceptors rather than donors. Once again, the minority dopants, in this case  $N_D$ , are compensated by the majority dopants. The ionized donor sites ( $N_D^+$ ) create a positive depletion width which requires applying a negative bias to the blocking layer contact. When the acceptors are ionized by incident light, the resulting hole is pulled along the valence band to the blocking layer contact, and the  $N_A^-$  carrier is pushed to the active layer contact. Again, this is the photocurrent collection method in a standard biased p-type BIB [6,7].

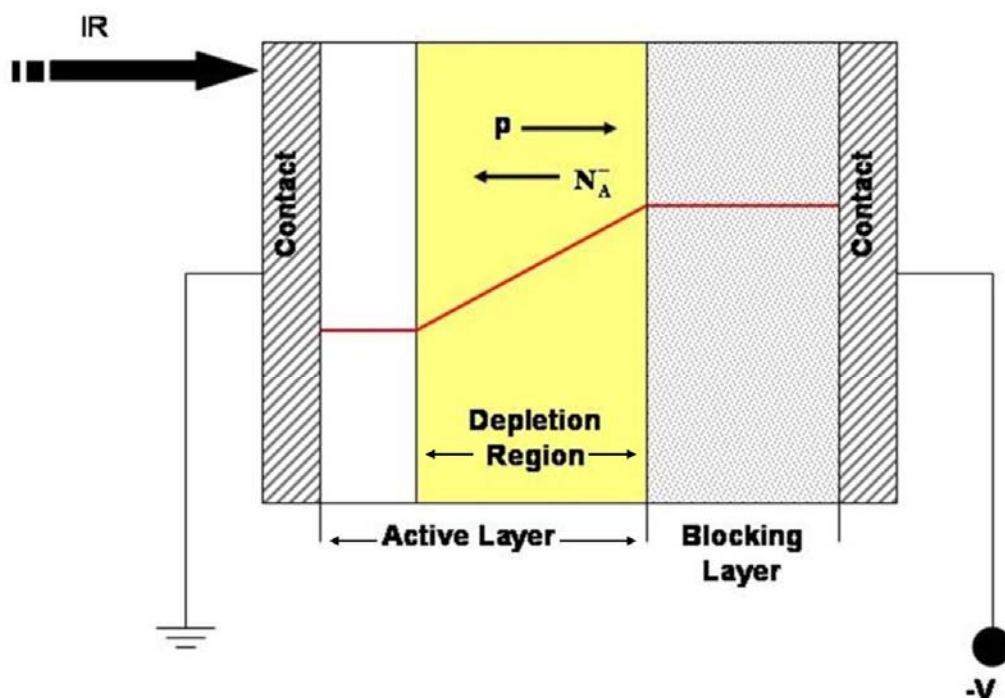


**Figure 3 Schematic diagram of standard biased p-type BIB. Red line indicates the electric field distribution.**

These two relatively simple, oppositely doped devices can result in a great deal of complexity, especially with the variety of currents and space charge that must be included in any analysis. The photogenerated majority carriers, dependent on the majority dopant, create the most obvious source of current, however the ionized majority dopant sites also create the hopping current. The minority dopant brings another charge to be considered, specifically for depletion regions, and drift and diffusion currents between the two layers and from the contacts must be included. The effects of these various charges lead to complex, sometimes counter intuitive results. Analysis of space charge effects, particularly in the blocking layer, on characterization techniques will be analyzed in depth in this thesis.

## II. EXPERIMENTAL SETUP

### A. COMPUTATION SETUP

All of the research into BIBs at the Naval Postgraduate School is computational modeling and device simulation. The computational model outputs 13 different variables for each iteration, and a single run generally requires fifteen to twenty thousand iterations depending upon the applied bias. This research required over 500 simulations which would not have been possible without several computationally powerful computers. The BIB lab consists of three machines with AMD (3000+) Athlon 64 Bit processors, Suse Linux 9.1 operating systems, and 2 GB 400 DDR RAM. Two of the computers have 80 GB hard drives, while the third has a 120 GB hard drive. Finally, the data analysis was performed on a fourth, Windows XP machine using Sigma Plot.

### B. FINITE DIFFERENCE COMPUTER MODEL

The three Linux computers run a finite difference, one dimensional model which calculates steady state values for the electric field, carrier concentrations, free carrier current, and ionized impurity band (hopping) current as functions of position. This model has been used previously to study field distributions in BIB devices [8,9]. The model arrives at these parameters by solving Poisson's equation, current continuity, and detailed balance in one dimension. This model is written to solve these equations for a p-type device, although it is simple to model n-type devices through sign adjustments to the model outputs.

Using Poisson's equation

$$\epsilon\epsilon_o \frac{\partial E}{\partial x} = q(p - n + N_d^+ - N_a^-) \quad (2.1)$$

it is possible to solve for the electric field E as a function of space charge. Here  $\epsilon\epsilon_o$  is the permittivity of the region, p and n are the concentrations of free electrons and holes at each position,  $N_D^+$  is the concentration of ionized donor sites, and  $N_A^-$  is the concentration of ionized acceptor sites. The ionized minority

population (for a p-type device  $N_D^+$ ) is treated as the minority doping  $N_D$  in the model due to compensation by the majority dopant. In the model, two mobile charge carriers are included in calculations, the majority carrier (for a p-type device free holes in the valence band) and the ionized majority dopant (ionized sites in the dopant/acceptor band).

The current continuity equations for positive and negative ionized charge carriers are

$$\frac{\partial p}{\partial t} = G - R - \frac{\partial J_p}{\partial x} \quad (2.2)$$

$$\frac{\partial n}{\partial t} = R - G - \frac{\partial J_n}{\partial x} \quad (2.3)$$

In these equations, G represents the generation rate and R represents the recombination rate of the free carriers. The generation rate can be defined as

$$G = (\gamma + \sigma v_p p_1) (N_A - N_A^-) \quad (2.4)$$

in which  $\gamma$  is the optical generation of free carriers and the second term represents the thermal generation rate. This second term comes from a detailed balance argument which requires the thermal emission rate from remaining neutral acceptor sites to equal the recombination current.

$$R = \sigma v_p p N_A^- \quad (2.5)$$

In relating these two equations,  $\sigma$  is the capture cross section of an ionized acceptor site,  $v_p$  is the effective speed of the ionized majority free carrier, and  $p_1$  is an unknown. To solve for this value, a new factor  $\alpha$  must be solved for in the relation between the thermal emission rate and the recombination current.

$$\alpha (N_A - N_A^-) = \sigma v_p p N_A^- \quad (2.6)$$

Here, at thermal equilibrium

$$p = N_v e^{\frac{-qE_F}{kT}} \quad (2.7)$$



in which  $N_V$  is the density of states in the valence band and  $E_F$  is the energy of the Fermi level above the valence band. The thermal equilibrium relationship between ionized and neutral acceptors is the Fermi relationship

$$\frac{N_A^-}{(N_A - N_A^-)} = \left(\frac{1}{4}\right) e^{\frac{q(E_F - E_A)}{kT}} \quad (2.8)$$

where  $E_A$  is the ionization energy of the acceptor dopant. Substituting Equations 2.7 and 2.8 into Equation 2.6 leads to the solution

$$\alpha = \sigma v_p \left(\frac{N_V}{4}\right) e^{\frac{-qE_A}{kT}} = \sigma v_p p_1 \quad (2.9)$$

which gives  $p_1$  as required for Equation 2.5.

$$p_1 = \left(\frac{N_V}{4}\right) e^{\frac{-qE_A}{kT}} \quad (2.10)$$

This allows one to relate the Generation and Recombination rates

$$G - R = (\gamma + \sigma v_p p_1)(N_A - N_A^-) - \sigma v_p p N_A^- \quad (2.11)$$

which must be zero for  $\gamma$  equal to zero per the assumptions made for the calculation.

Referring back to the continuity equations (Equations 2.2 and 2.3) equations for  $J_n$  and  $J_p$  are also required. These currents are the combination of both diffusion and drift currents for electrons and holes.

$$J_n = qD_n \frac{\partial n}{\partial x} + q\mu_n n(x)E(x) \quad (2.12)$$

$$J_p = qD_p \frac{\partial p}{\partial x} + q\mu_p p(x)E(x) \quad (2.13)$$

The drift components of these currents include the hopping current of the region, and to solve for this the model uses an analytical expression for the mobility of these ionized acceptors. The model assumes the simplified case of uniformly spaced dopants

$$\mu = \mu_0 x^{3.5} e^{-x} \quad (2.14)$$

$$x = 2 \left[ N_A^{1/3} a_B \right]^{-1} \quad (2.15)$$

with mobility treated as a function exponentially dependent on the Bohr radius  $a_B$ , the majority dopant concentration  $N_A$ , and a temperature dependent pre-factor  $\mu_0$  [10].

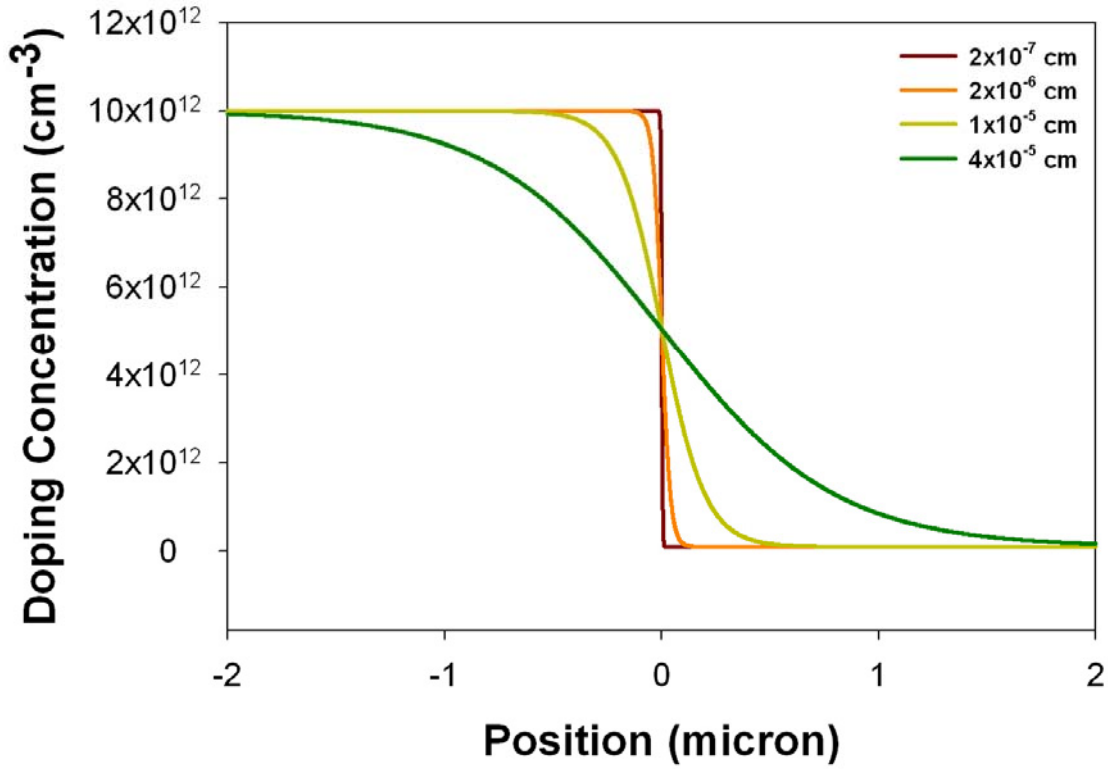


**Figure 4 Plot of doping profile as a function of position for four values of grade parameter ( $g$  from equation 2.16).**

Finally, in defining the entire device, the model includes smooth transitions between layer dopings through the use of an empirical hyperbolic function.

$$N = \frac{N_1 + (N_2 - N_1)}{1 + e^{[(a-x)/g]}} \quad (2.16)$$

Here, the doping concentration at any given point on an interface is a function of the doping  $N_1$  in the previous region, the doping level  $N_2$  in the next region, the

position  $a$  of the interface, the current position  $x$ , and the grading parameter  $g$  which is set prior to running the program. Figure 4 shows the effects varying this grade parameter has on the doping concentration transition between different layers [8].

Employing this powerful set of equations requires an extensive input of variables to define the characteristics of the BIB device to be modeled. Figure 5 shows an example of these input files with many of the key parameters labeled.

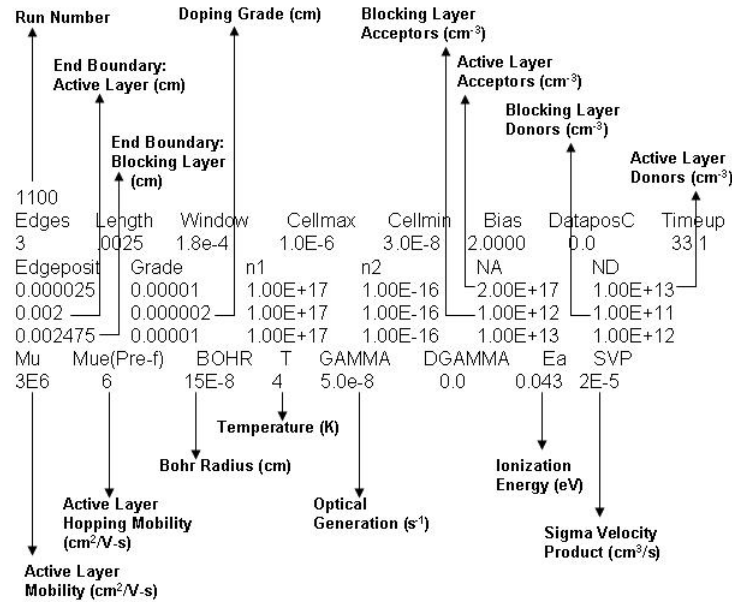


**Figure 5 BIB input file**

The model treats the BIB as a four layer device, so all of these layers must be defined in the input file. The two contacts are treated as heavily doped ohmic regions which supply free carriers at all temperatures. In a p-type device the model treats the BIB as a system with free holes and ionized acceptors, so the contact is assumed to supply holes. Usually the contacts are assigned thicknesses of  $0.25 \mu\text{m}$ . As seen in Figure 5 the active layer and the blocking

layer can also assume whatever thickness is desired. The majority and minority dopant concentrations are assigned to each region, and the grades between these values can be assigned for all three interfaces in the device.

The input file also allows for defining different host materials, and these variables include the mobility of free carriers, the mobility of ionized acceptors (ionized majority dopants), the Bohr radius  $a_B$ , the majority dopant ionization energy, and the cross section velocity product  $\sigma v_p$ . All of these material parameters are listed on the bottom line of the input data file.

Finally, the input file includes individual run specific variables such as the operation temperature in Kelvin, the Optical Generation rate  $\gamma$  which is a measure of the flux on the device, and the bias applied to the device.

The model takes this input file of the BIB characteristics and calculates the 13 variables shown in Figure 6. It arrives at this solution by stepping up the applied bias from zero to the input file value in steps of 0.01 mV. It arrives at a steady state solution for each position at a set bias, and then using the previous solution and new values solves for the next slightly higher bias. The final output file is the value of all the variables at each incremental position in the device, for the final bias provided on the input file.

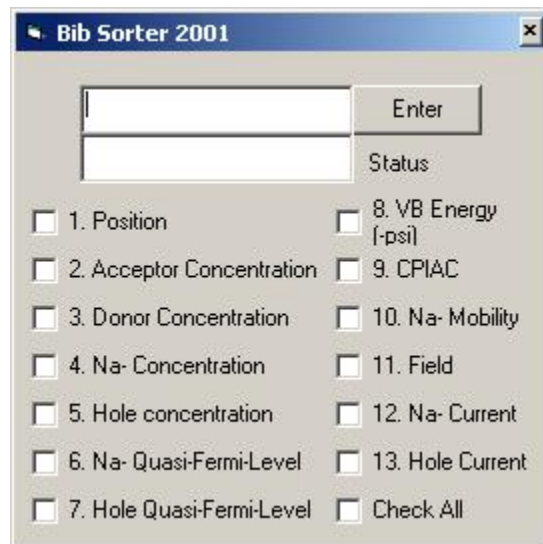


**Figure 6 BIB output file**

Achieving a timely solution in BIB modeling is often dependant upon how the problem is defined. Each increment of 0.01mV requires a large number of iterations as the program steps through the device. The length of the device and complexity (doping concentrations and grade parameters) will determine how large or small the total number of iterations will be. Likewise, the lower the temperature and the optical flux values, the more iterations required. Simulations for Si BIBs tend to run significantly faster than those for GaAs or Ge BIBs due to more ideal field distributions. The end result is that a solution can be completed in a matter of minutes or in weeks. Usually approximations can be made to reduce the time required to complete a simulation, however the model allows for highly accurate, and time consuming, calculations when the need exists.

THIS PAGE INTENTIONALLY LEFT BLANK

### III. C-V PROFILING METHOD

#### A. GROWTH CONSTRAINTS

Challenges of growing extremely thin, high purity, and low compensation materials are currently limiting the extension of BIBs into the far-infrared regime. Minority doping levels in the active layer are of critical importance and pose a special challenge in the growth of compound semiconductors such as GaAs. Because the depletion width in the active layer is a function of the compensation, the depletion widths become prohibitively small as compensation levels get too high. This can be seen in Figure 7, which compares two GaAs BIBs, one with 0.1% compensation and the other with 10% compensation in the active layer.

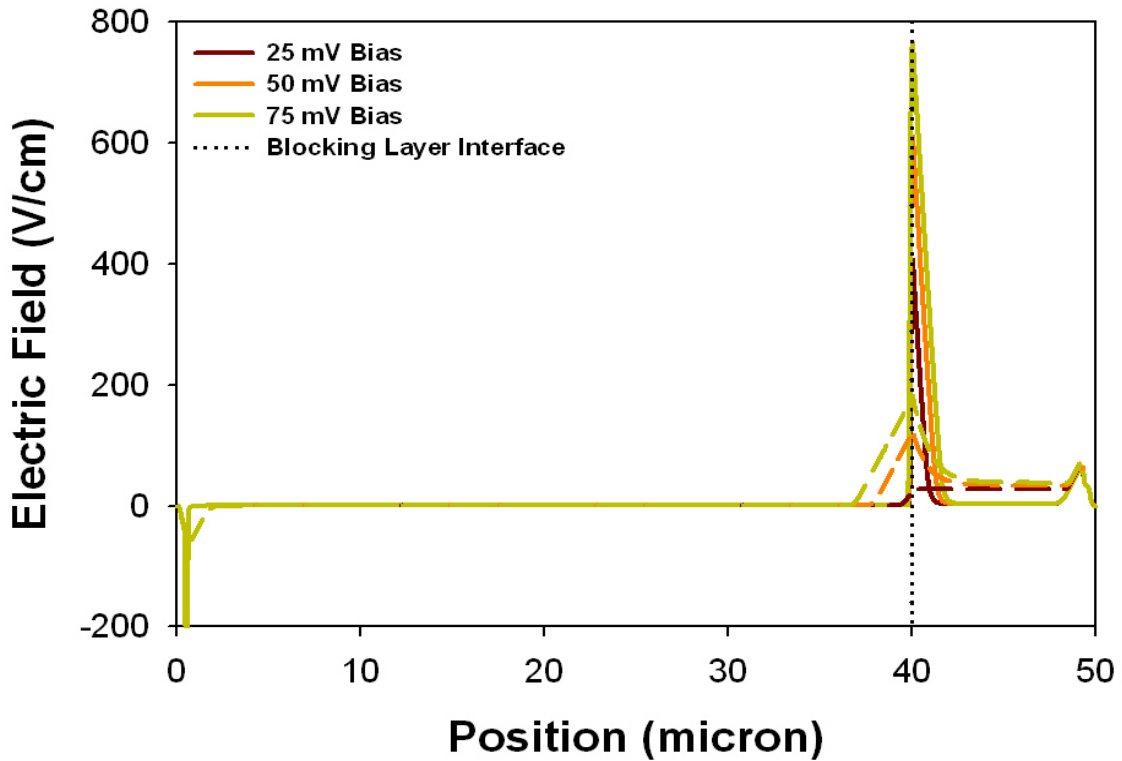
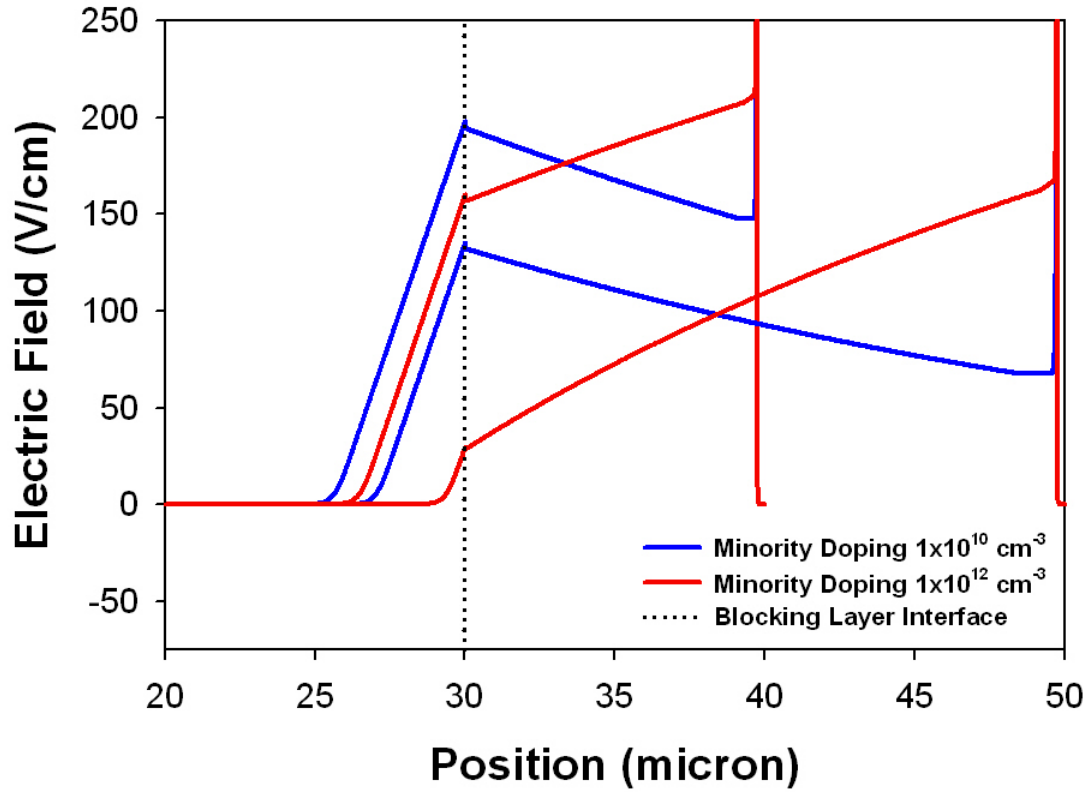


Figure 7 Active layer compensation effects in GaAs (solid line 0.1%, dashed line 10% compensation)

For the case with a compensation of 0.1%, the device would function as a BIB photodetector because the depletion width extends into the active region due to the lower compensation. As a result the photocurrent from ionized carriers in the depletion region could be collected. The second compensation of 10% is so large the depletion region shrinks to nothing, and any photo-ionized carriers in the active layer will recombine rather than be collected as photocurrent.

Difficulties in achieving extremely thin, pure blocking layers also raise minority doping issues. The blocking layer ideally has an extremely low minority doping level to minimize space charge effects. In addition compensation should be minimized such that as little field is dropped in the layer as possible. This material constraint can be difficult to attain, and in the case of Ge significant grading in the blocking layer active layer interface requires a thicker layer to allow the doping levels to transition to the required purity level. Figure 8 illustrates these difficulties as the depletion width decreases significantly with both thicker blocking layers and with higher compensation levels.





**Figure 8 Electric field profiles for varied blocking layer thicknesses (10 and 20  $\mu\text{m}$ ) and minority doping levels in a Ge BIB.**

Common to both of these situations is the importance of knowing and then controlling compensation levels throughout the BIB device for the development of longer wavelength response BIBs. Certainly the difficulty of controlling compensation levels can be attributed to many factors, but the assumptions and error in measurement techniques adds to an already complex problem [11,12].

#### **B. C-V PROFILING METHOD THEORY**

In isolated bulk samples or epitaxial layers, compensation levels are generally measured using variable temperature Hall effect. The minority doping concentration affects the statistics of recombination and causes variations in slope of the majority carrier “freeze-out” curve. However, this technique can generally not be applied to layers within a multi-layer structure. A different approach is therefore required to measure BIB material parameters within the device structure.

The current technique used to measure compensation in Blocked Impurity Band Detectors is a low temperature application of the C-V profiling method. C-V profiling involves measuring the change in capacitance of the active layer in a BIB detector for a very small change in applied bias. An initial bias is applied to the device such that the depletion width extends into a region where the doping characterization is desired. A slight voltage variation is applied, and the change in capacitance of the device is measured. Using this  $\Delta C$  and the small change in voltage, the doping-related space charge in the region can be calculated [13].

In standard C-V profiling, we assume that the minority dopant sites are compensated by the majority dopants and the temperature of the device is high enough to allow free movement of the majority carriers. When the depletion width is established for this case, the total space charge remaining is a combination of both the ionized majority and minority dopant sites,  $N_{\text{maj}} - N_{\text{min}}$ . The majority concentration is significantly higher than the minority concentration, so this method is used to measure net majority doping in devices. For the low temperature variation the minority dopants are once again compensated, but the low thermal energy causes the majority carriers to be bound to their dopant sites. The result is that the space charge in the depletion region arises from only minority dopants.

This low temperature C-V profiling method begins with the approximation that within the depletion width the space charge is proportional to the minority doping concentration  $N_D$

$$\rho \cong qN_D \quad (3.1)$$

From this approximation the depletion width can be calculated.

$$W = \sqrt{\frac{2\epsilon_s}{qN_D} \left( V_{bi} - V - \frac{kT}{q} \right)} \quad (3.2)$$

In this equation  $V_{bi}$  is the built-in potential,  $V$  is the applied potential, and the term  $\frac{kT}{q}$  takes into account the majority-carrier distribution tail. Multiplying the

space charge with the depletion width, Equation 3.1 with 3.2 gives the total space charge in the depletion region.

$$Q_{sc} = \sqrt{2\epsilon_s q N_D \left( V_{bi} - V - \frac{kT}{q} \right)} \quad (3.3)$$

The derivative of Equation 3.3 with respect to change in bias voltage allows for the calculation of the capacitance.

$$C = \frac{|\partial Q_{sc}|}{\partial V} = \sqrt{\frac{q\epsilon_s N_D}{2 \left( V_{bi} - V - \frac{kT}{q} \right)}} \quad (3.4)$$

The desired parameter is the minority concentration, so Equation 3.4 can be manipulated

$$-\frac{d(1/C^2)}{dV} = \frac{2}{q\epsilon_s N_D} \quad (3.5)$$

such that the minority concentration can be isolated.

$$N_D = \frac{2}{q\epsilon_s} \left[ -\frac{1}{d(1/C^2)/dV} \right] \quad (3.6)$$

Experimental determination of  $N_D$  requires two measurements of capacitance at slightly different applied biases. This surprisingly simple solution hides several important assumptions. The starting point of the calculations is the assumption that all the space charge is in the active layer, and that the space charge consists exclusively of ionized minority sites. Most significant of these assumptions is that the blocking layer purity is high enough to ignore any space charge in the layer.

The goal of this work is to perform numerical simulations of the C-V method that include space charge in the blocking layer and at the active layer/blocking layer interface. This will allow for simulation of and interpretation of C-V data outside the range of the restricting assumptions described above.

THIS PAGE INTENTIONALLY LEFT BLANK

## IV. MODELING RESULTS

### A. LOW TEMPERATURE C-V MODELING

The question of space charge in the blocking layer lends itself perfectly to application of computer simulation. Whereas in actual devices space charge cannot be directly measured on a point-by-point basis, the model calculates values for all the parameters shown in Figure 6 for finite steps through the device. It is therefore a simple matter of extracting and plotting the data to see the equilibrium space charge distribution in a given device configuration. Figure 9 shows an example of this space charge profile throughout a BIB device. The values between 11 and 17  $\mu\text{m}$  are plotted in blue to indicate that the space charge changes sign in this region. Most importantly, the data is continuous across the device.

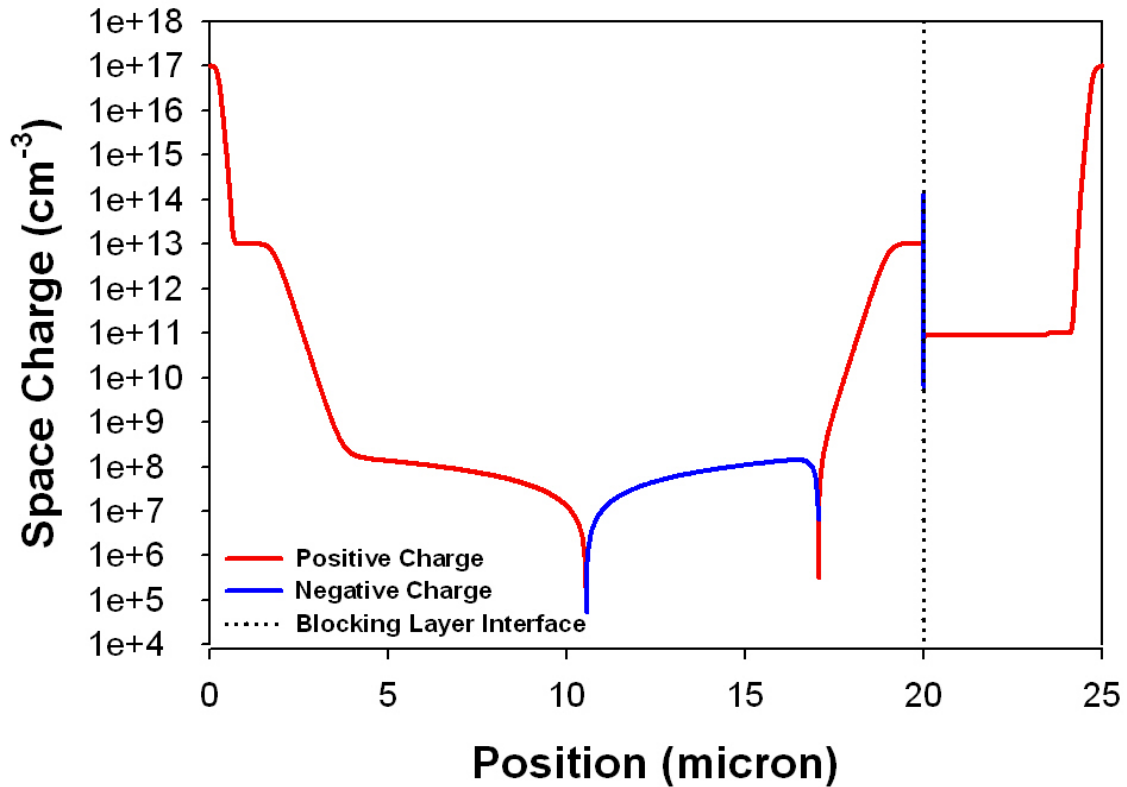
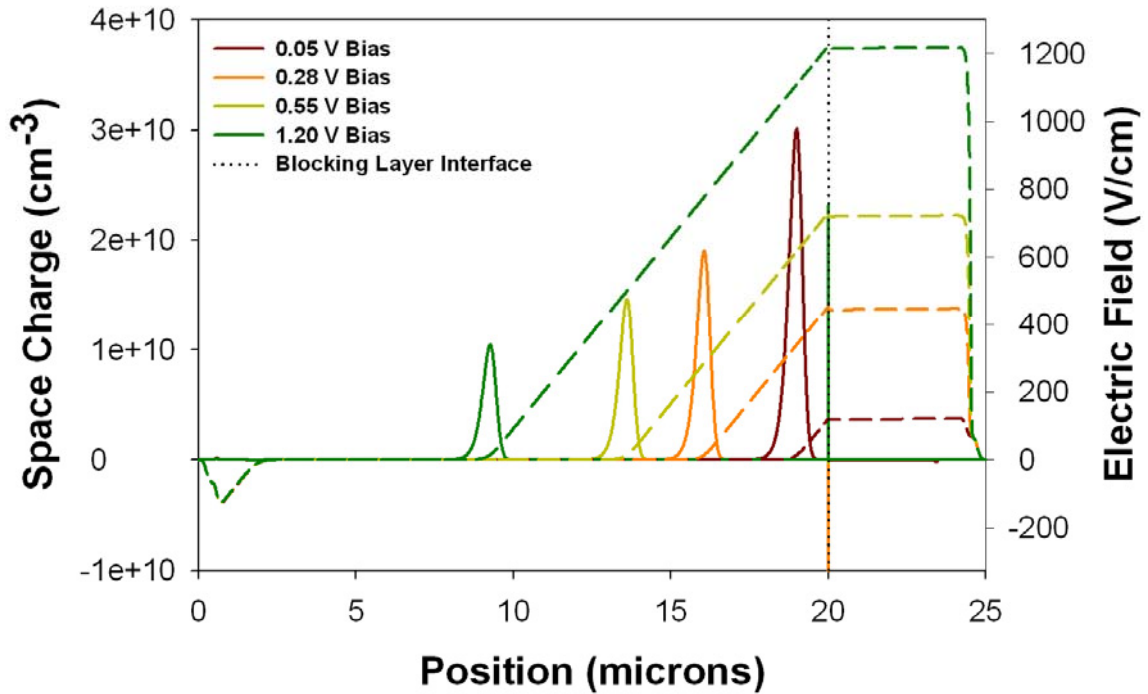


Figure 9 Space charge profile for a Si BIB with a 0.05 V Bias (Table 1).

The natural point to begin modeling the low temperature C-V profiling method is therefore to solve for capacitance, Equation 3.4, using the full spatially determined space charge ( $Q_{sc}$ ) for a given bias. This means we no longer need to tolerate the approximation, Equation 3.3, that the minority doping in the active layer constitutes all the space charge. Solving for capacitance at any point in the device requires two space charge profiles. These must be subtracted to solve for a change in space charge ( $\partial Q_{sc}$ ) over a small change in bias ( $\partial V$ ). In the computer simulations, the small change in bias was kept constant at 0.1 mV. Subtracting the two space charge profiles gives both the magnitude and the distribution of the change in space charge. By applying this method for multiple biases, it is possible to probe through the device as shown in Figure 10.



**Figure 10** Modulated change in space charge (left axis, solid) and electric field (right axis, dashed) as a function of position for a case with an ideally sharp interface.

Absorbing Layer Majority Doping	$2.0 \times 10^{17} \text{ cm}^{-3}$
Absorbing Layer Minority Doping	$1.0 \times 10^{13} \text{ cm}^{-3}$
Absorbing Layer Thickness	$20 \text{ } \mu\text{m}$
Blocking Layer Majority Doping	$1.0 \times 10^{12} \text{ cm}^{-3}$
Blocking Layer Minority Doping	$1.0 \times 10^{11} \text{ cm}^{-3}$
Blocking Layer Thickness	$5 \text{ } \mu\text{m}$
Temperature	4 K
Bohr Radius	$15 \times 10^{-8} \text{ m}$
Contact Grade Parameter	$1.0 \times 10^{-5} \text{ cm}$
Optical Flux Rate $\gamma$	$5.0 \times 10^{-8} \text{ s}^{-1}$ for Photo-Current

**Table 1 Si BIB parameters used for C-V simulations**

The idealized case in Figure 10 has the device parameters shown in Table 1, with a sharp grade ( $g=2 \times 10^{-7} \text{ cm}$ ) between the active layer and blocking layer. Slight variations in device parameters will be made throughout this section, but they will be referenced back to these general conditions. In Figure 10, it is apparent that the change in space charge occurs almost entirely at the outer boundary of the depletion region. Integrating this space charge results in the total change in space charge, and this can be inserted into Equation 3.4 to solve for the capacitance. For the range of bias voltages initially selected it is now possible to produce a plot of  $1/C^2$  versus  $V$  (Figure 11). The minority doping concentration is proportional to the inverse of the slope of  $1/C^2$  as seen in Equation 3.6. The active layer minority doping level shown in Table 1 for this idealized case matches the calculated values.

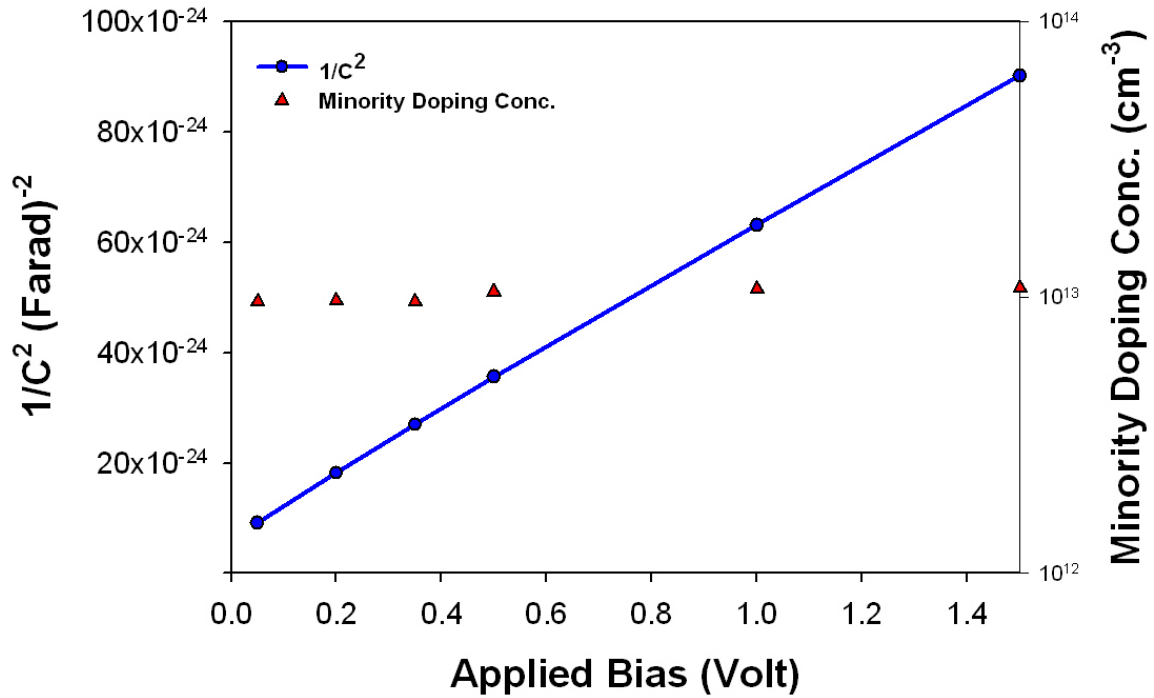


**Figure 11  $1/C^2$  and minority doping as a function of applied bias. Parameters listed in Table 1.**

One adjustment has been made in the simulation results shown, and this is due to capacitance changes in the immediate contact areas. Free carriers in the contacts diffuse into the device and recombine over a given distance setting up a space charge region known as a Debye tail. The space charge in this region also changes with the bias, as seen in Figure 12. Due to its higher concentration of carriers, the Debye tail will have a lower resistivity than the rest of the device. This lower resistivity region will also have a smaller RC time constant. In experiments contact effects are therefore removed with other parasitic effects by subtracting a higher frequency  $\Delta C$ . In simulations, the model outputs the total spatial variation of the change in space charge, so this high frequency subtraction can be accounted for by setting near contact values equal to zero.



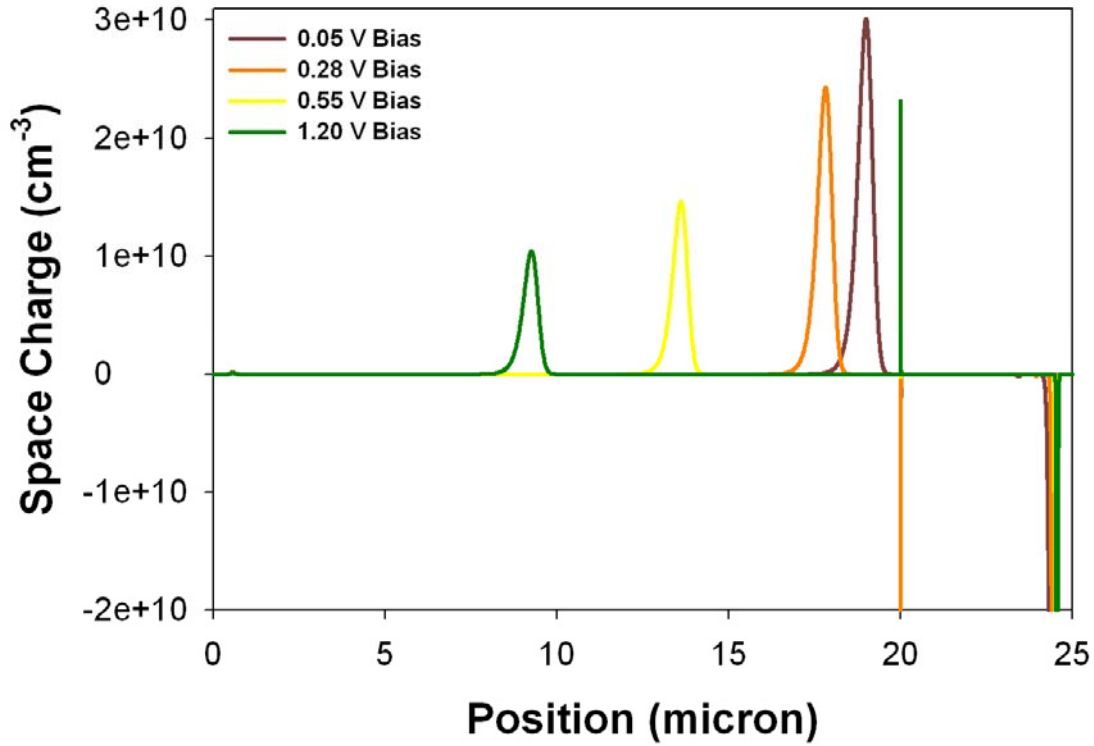


**Figure 12 Space charge variations that include near contact space charge (far right). Parameters listed in Table 1.**

## **B. INTRODUCING INTERFACE GRADES**

The result of the calculations shown in Figure 11 demonstrates that low temperature C-V profiling is accurate for cases that match the assumption of a high purity, space charge free blocking layer. The focus of this research is to investigate the effects of space charge in the blocking layer on the C-V profiling method, with the goal of determining if it could be responsible for unexpected profiling results. Figure 13 shows one such result from a Raytheon Vision Systems profiling run on material for Si:As BIBs [14].

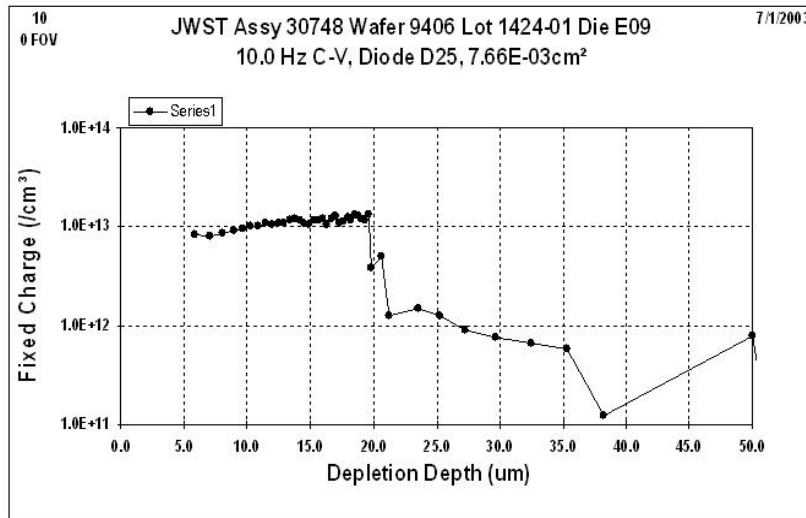


**Figure 13 Low temperature C-V profiling results (Courtesy of P. Love).**

The grade between doping levels at the active/blocking layer interface plays a significant role in the buildup of space charge, so including this parameter in the modeling is very important. As discussed earlier, one of the difficulties with growing thin pure blockers is that the doping levels do not decrease rapidly enough from heavily doped to highly pure. Instead, a transition region exists where the material properties are intermediate. Figure 14 shows one such transition region as measured with a spreading resistance probe for a Si:As BIB. Starting from the left side of the plot, the blocking layer has a doping level of  $2 \times 10^{13} \text{ cm}^{-3}$  at the furthest point from the active/blocking layer interface, but clearly this does not characterize the entire blocking layer. In fact,  $2 \mu\text{m}$  into the layer the doping level has already transitioned to  $1 \times 10^{14} \text{ cm}^{-3}$ . This characteristic must be taken into account to fully understand device performance [14].

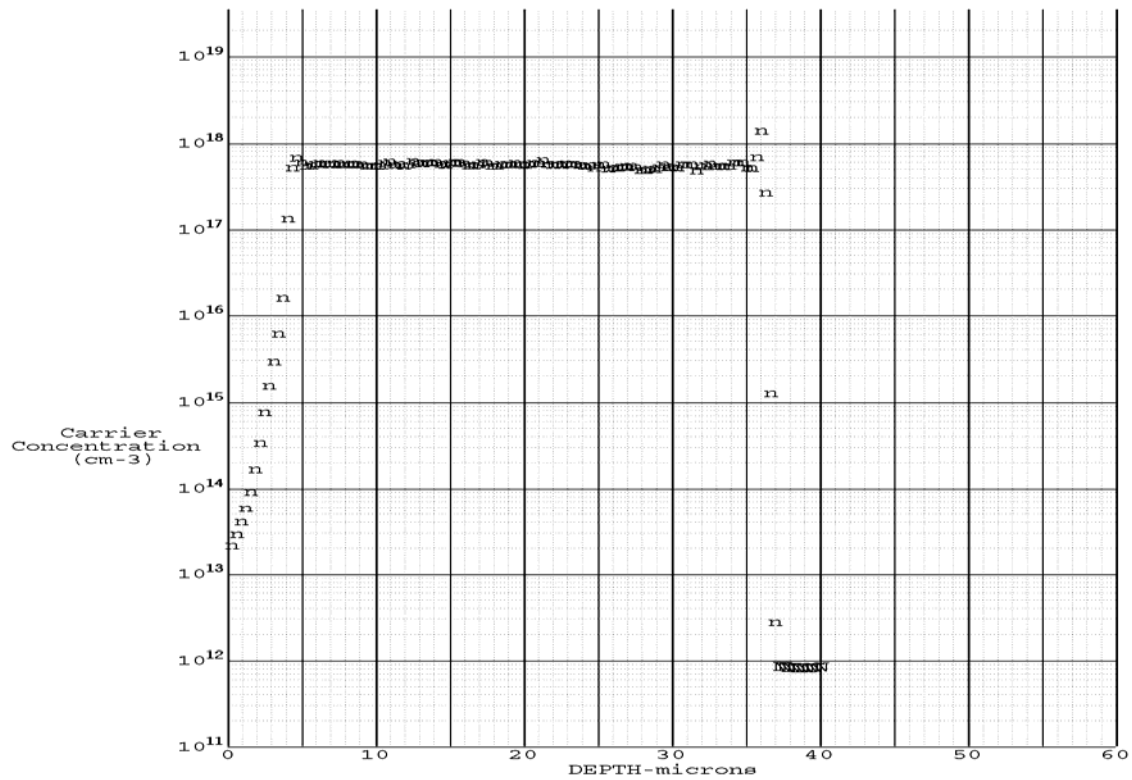


**Figure 14 Spreading resistance measurement showing graded region, blocking layer starting from the left, active layer  $\sim 5 - 35 \mu\text{m}$  (Courtesy of P. Love).**

The graded region is modeled in the program as previously shown in Figure 4, allowing variation of the extent of this transition region. The first step taken which included the grade was to model a simplified case with minimal space charge variation between the two regions. In this case, the graded region was set to a very gradual grade parameter of  $g=2 \times 10^{-5} \text{ cm}$ , and the majority doping concentration was held constant at  $2 \times 10^{17} \text{ cm}^{-3}$  across the entire device such that the only doping variation was in the minority doping level. Minority doping levels were set to  $1 \times 10^{13} \text{ cm}^{-3}$  in the active layer with a graded transition to  $5 \times 10^{12} \text{ cm}^{-3}$  in the blocking layer with all other parameters the same as shown in Table 1. Once again a range of biases were chosen and a set of two simulations were run for each bias, one 0.1 mV higher than the other. Figure 15 shows that the compensation calculations closely follow the expected transition from the blocking layer value of  $5 \times 10^{12} \text{ cm}^{-3}$  across the graded interface to the active layer value of  $1 \times 10^{13} \text{ cm}^{-3}$ .

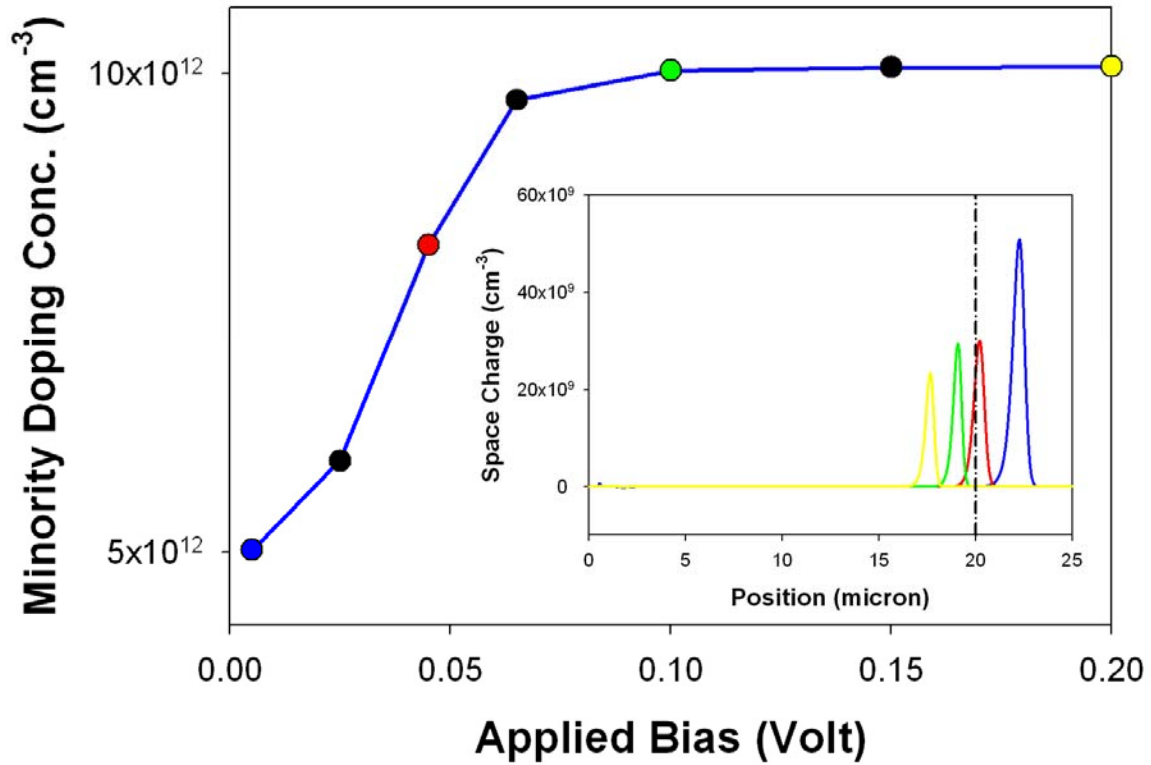


**Figure 15** Minority doping concentration as a function of bias for  $g=2 \times 10^{-5}$  cm. Inset depicts the actual position of space charge, and therefore the minority doping sample area, for several biases.

### C. REALISTIC DEVICE PARAMETERS WITH GRADE

The previous case showed that the low temperature C-V profiling method should work in a case with doping variation but also minimal space charge in the blocking layer and at the interface. We now repeat the simulations from the previous section, but for a case in which the majority doping in the blocking layer is reduced to a realistic  $1 \times 10^{12} \text{ cm}^{-3}$  and the minority doping is reduced to  $1 \times 10^{11} \text{ cm}^{-3}$  (all Table 1 values). Changing the blocking layer majority doping alters the space charge distribution, and the role of the grade between the blocking layer and the active layer becomes significant. Figure 16 and Figure 17 demonstrate the effects of varying grade parameters on C-V results for otherwise identical structures.

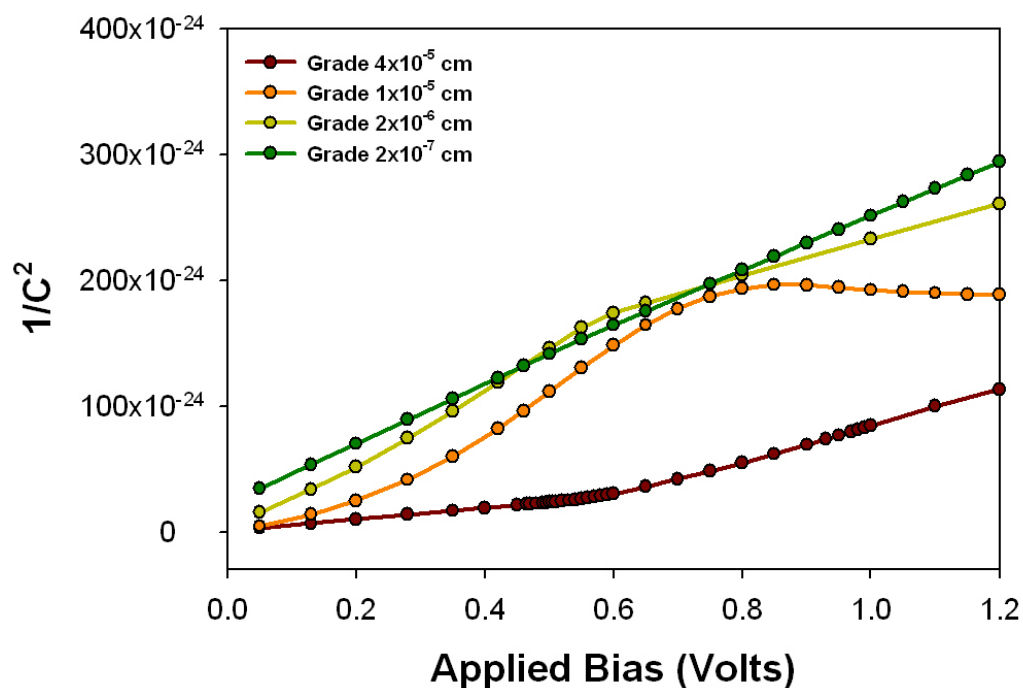


Figure 16  $1/C^2$  as a function of applied bias. Parameters listed in Table 1 with varied interface grade.

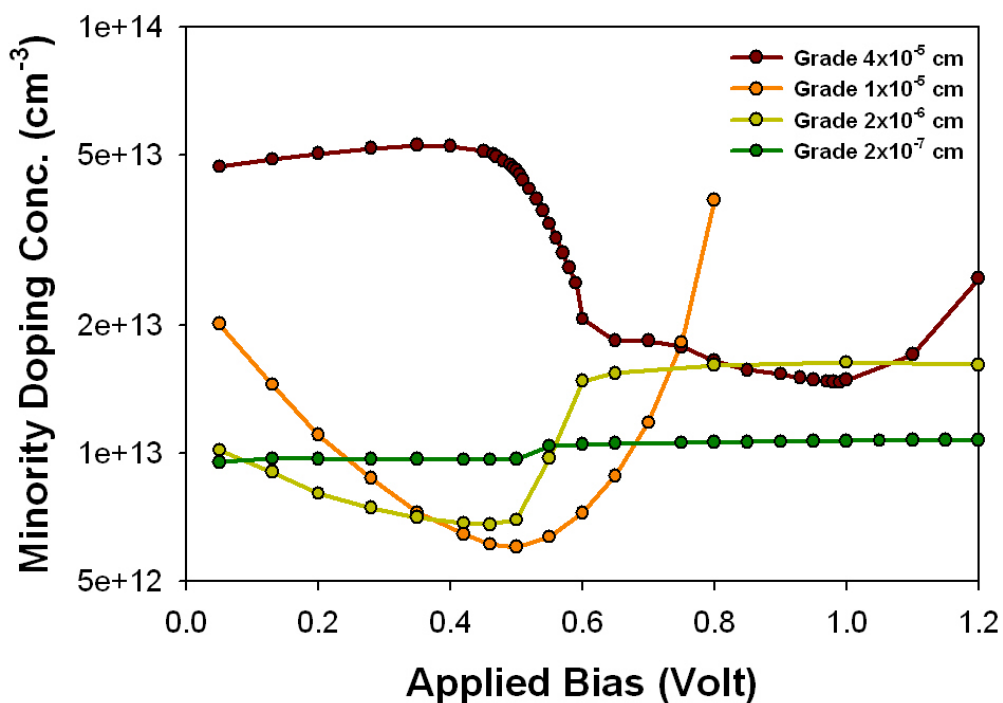


Figure 17 Compensation calculations from C-V profiling, calculated from Figure 16, as a function of the applied bias. Parameters listed in Table 1 for varied interface grade.

For the case with the sharpest grade,  $g=2 \times 10^{-7}$  cm, the calculated minority doping concentration as seen in Figure 17 is almost exactly the actual simulated doping level of  $1 \times 10^{13}$  cm<sup>-3</sup>. It remains consistent at this level as the depletion width is varied. As the grade is increased, the calculated values from the initial part of the curve for the initial bias increase steadily. In addition the plots begin to show surprising step functions and variations at higher biases. These results show similar characteristics to the experimental results shown in Figure 13.

It is clear that space charge in the blocking layer and at the active layer/blocking layer interface affects calculations of minority doping concentration. Standard interpretation of the C-V profiling method ignores any space charge in the blocking layer. It assumes that small changes in the applied bias will change the electric field profile only at the end of the depletion width in the active layer. This is a safe assumption for the idealized cases initially discussed which include uniform layers, layers with very similar doping levels, or layers with different doping levels sharply graded at the interface. However, in non-ideal cases, particularly when a grade is introduced, this is no longer a valid approximation as seen in the strikingly similar results of the simulations, Figure 17, and the experimental results, shown in Figure 13. The next step is to determine why the space charge causes such non-linear results.

#### **D. ANALYSIS**

When the blocking layer ceases to be ideal, the device begins to behave like two separate depletion regions; changes in the electric field occur both at the anticipated point near the end of the depletion width in the active layer and in the blocking layer due to local space charge. This double depletion effect is most evident as the grade parameter is increased. For the largest grade parameter,  $g=4 \times 10^{-5}$  cm, Figure 18 shows the space charge variation in both layers. Clearly, in this case the assumption of a space charge free blocking layer ceases to be valid. The leap from the blocking layer space charge profiles seen in Figure 18 to the minority doping calculations seen in Figure 17 is complex and requires an

in-depth look at what is actually happening in the blocking layer and at the active layer/blocking layer interface.

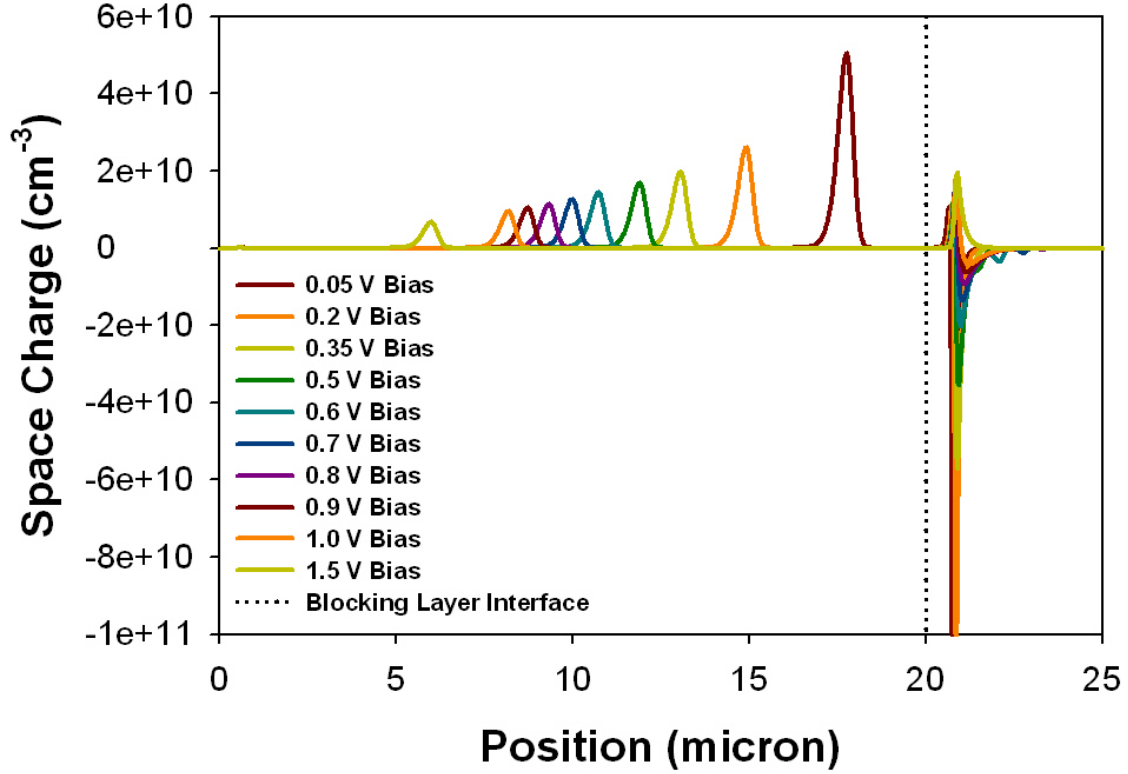


**Figure 18** Change in space charge as a function of bias for grade  $g=4 \times 10^{-5}$  cm.

The best starting point is an analysis of the change in space charge ( $\partial Q_{sc}$ ) profiles in the active layer, which have already been introduced and explored in Figure 10. Each  $\partial Q_{sc}$  profile is a result of the corresponding 0.1 mV change in applied bias between the two simulated runs. In the active layer the total  $\partial Q_{sc}$  between each set of biases decreases as the overall bias is increased. This occurs because the relationship is nonlinear, and the capacitance ( $\partial Q_{sc} / \partial V$ ) varies as a function of  $1/\sqrt{V}$  (Equation 3.4). The 0.1 mV variation no longer

causes as large an increase in  $\partial Q_{sc}$  at higher bias, so the measured capacitance decreases with bias, and  $1/C^2$  increases, in the ideal case, linearly with  $V$ .

This is crucial to understanding the calculation of the minority doping concentration. It requires that the derivative of  $1/C^2$  be positive for the calculated minority doping to be positive (Equation 3.6). The only way this can occur is if the total  $\partial Q_{sc}$  decreases as the applied bias increases. One ramification of this is that the extracted minority doping concentration approaches infinity if the slope of  $1/C^2$  transitions from positive to negative. This can be seen in Figure 16 and Figure 17 for the  $g=1 \times 10^{-5}$  cm grade. The slope of  $1/C^2$  approaches zero and becomes negative and the calculated minority doping approaches positive infinity before becoming a negative (meaningless) number.

A straightforward physical description of the results seen in Figure 16 and Figure 17 is difficult because the nonlinear results arise from multiple interrelated factors. These factors are

- a. the change in the effective bias in the active layer resulting from blocking layer space charge,
- b. the change in total space charge because of blocking layer space charge magnitudes,
- c. the spatial variation of the graded dopant concentrations.

These factors help in understanding three key features in Figure 17:

1. variation in predicted value with grade,
2. negative slope in  $1/C^2$  leading to negative calculated doping levels,
3. step functions in calculated doping levels.



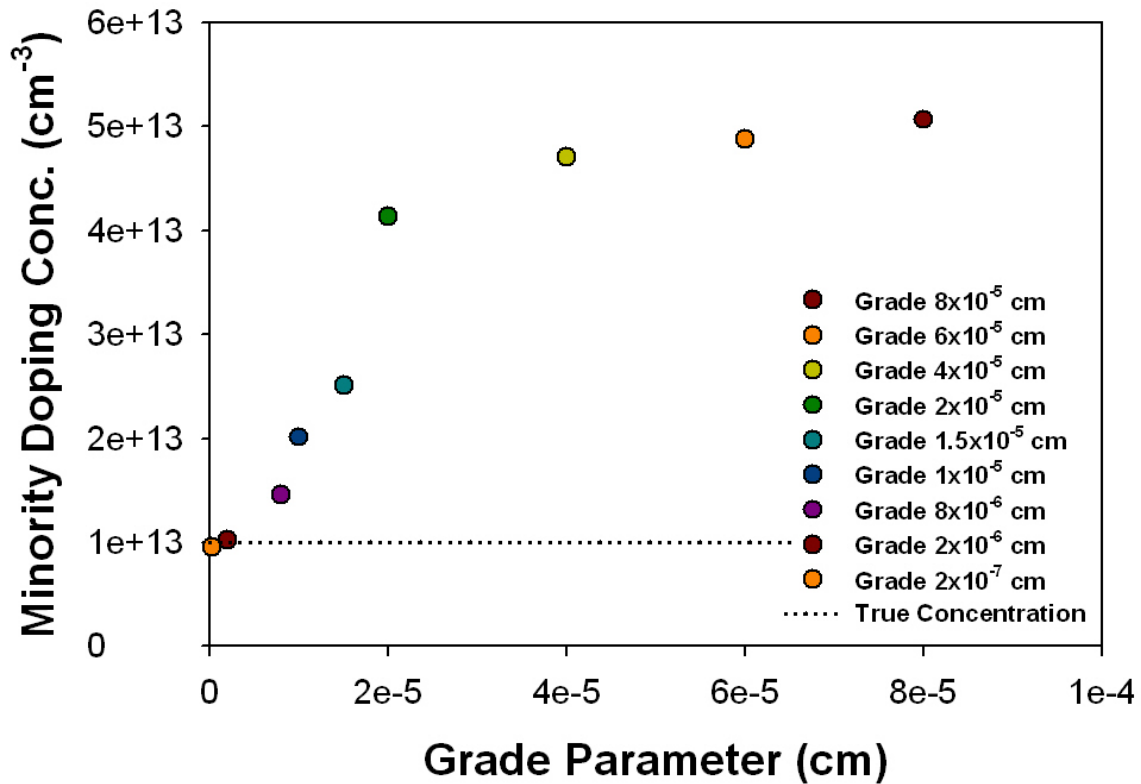


**Figure 19 Grade effects on initial (0.05 V) calculated minority doping.**

Starting with the variation in the predicted value as a function of grade (1), Figure 19 shows the overall increase in calculated doping level as the grade increases, for the lowest bias used. Although the calculated value deviates further from the actual value as the grade is increased, the effect is clearly nonlinear. Figure 20 shows the expanded field profiles of several of these runs at the interface for increasing grade between the active and blocking layer. The change in field at the interface is a function of the increase in grade between the two regions. At this low bias, positive space charge in the blocking layer immediately adjacent to the active layer is responsible for a significant field variation at the interface.

One effect of this positive space charge is to increase the field at the interface, thereby increasing the overall extent of the depletion width into the active layer, as shown. Adjusting the amount of space charge in the blocking layer will therefore change the depletion width, resulting in an overall change in

the total bias dropped in the active layer. The slight 0.1 mV increase in bias causes a change in space charge in the blocking layer. This in turn changes the overall depletion width into the active layer from what it would have been for a 0.1 mV increase in bias with no blocking layer variation. The resultant  $\partial Q_{sc}$  in the active layer behaves as if a different bias had been applied (a). This changes the measured capacitance from what it would have been without the blocking layer space charge, and explains why the extracted values of minority doping concentration at low biases increase for increased grades.

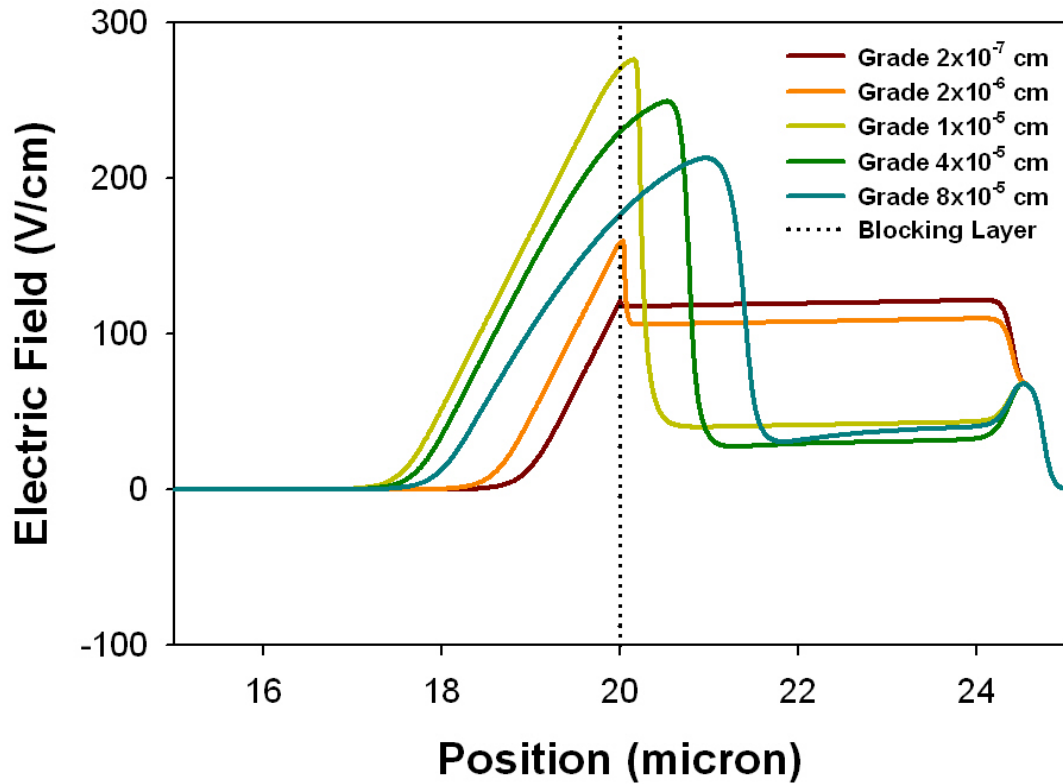


**Figure 20 Expanded field profiles near the interface at 0.05 V bias, varied grade parameters.**

Returning to the  $\partial Q_{sc}$  profiles in Figure 18 it is important to look closely at the characteristics in the blocking layer, detailed in Figure 21. First, there is significant negative change in space charge for the lowest bias of 0.05 V (decrease in positive space charge). This negative change will cause an overall

decrease in field from the case with no change. At the next bias, there is still a negative change, but it is smaller so the overall decrease in field will be smaller than for the first case. The result is that the change in space charge in the active layer is larger than it would have been without the blocking layer effects, which causes a smaller  $1/C^2$  slope and an increased minority calculation. These effects are nonlinear with grade as seen in Figure 19 and explain why the initial calculated minority concentrations increase as the grade increases.

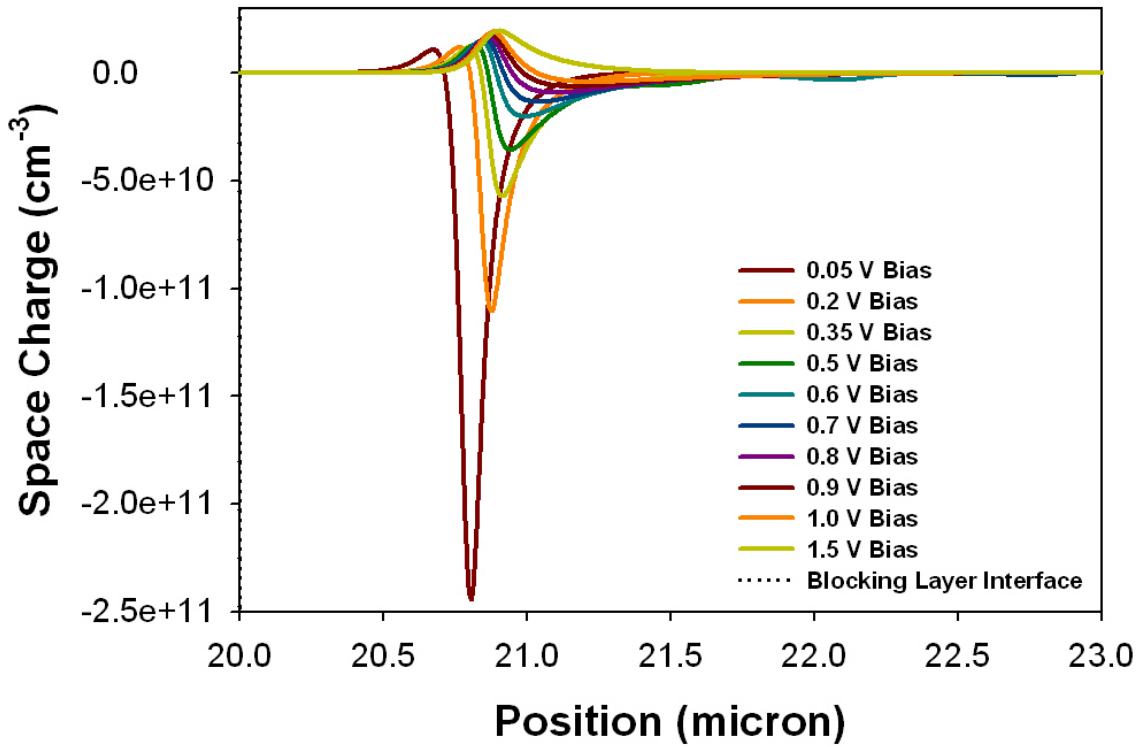


**Figure 21 Change in space charge in the blocking layer, grade  $g=4 \times 10^{-5}$  cm.**

The next key feature in Figure 17 is the rapid increase and then sign change in the minority doping calculations (2). This characteristic occurs for the  $g=4 \times 10^{-5}$  cm case in Figure 17 and correlates to the transition to a negative  $1/C^2$  slope in Figure 16. As previously discussed, a negative calculated minority calculation occurs when the change in  $\partial Q_{sc}$  becomes positive, so it is expected that  $\partial Q_{sc}$  steadily decrease as the depletion width extends further into the device. In Figure 17 the  $g=4 \times 10^{-5}$  cm case becomes negative at 0.8 V as a result of this

second factor, the absolute magnitude of space charge in the blocking layer (b). Looking at the space charge profiles in Figure 18 and Figure 21, it can be seen that the  $\partial Q_{sc}$  in the blocking layer increases with increased bias once it becomes positive. It becomes a more and more significant portion of the total  $\partial Q_{sc}$  in the device until finally at 0.8 V it represents a larger increase than the decrease in the active layer, and the net change is positive. This represents a total breakdown of the assumptions made in the standard method.

The last key feature, and most complex, is a simulated step function in the calculated minority doping (3). This feature combines the two factors already discussed, variation of the effective change in bias in the active region (a) and the absolute magnitude of the space charge in the blocking layer (b), with the third factor (c). This last factor is the grade's significant minority dopant variation (c), which can also be seen in Figure 20. It changes the fields from straight line approximations as in the sharpest case ( $g=2 \times 10^{-7}$  cm) to the wider curves pulled further into the blocking layer for the most gradual case ( $g=8 \times 10^{-5}$  cm). The net result is another level of complexity and nonlinearity not included in the low temperature C-V profiling approximation of minority doping.

The majority of the data seen in Figure 17 represents the combined effects of all of the factors listed. This coupling of the many blocking layer space charge effects leads to the nonlinear results seen, and variations cannot be easily attributed to any one cause. Most importantly, this result exposes the dangers of ignoring space charge in the blocking layer when calculating minority doping concentrations, particularly when graded regions are introduced. The combined effects of blocking layer space charge on the depletion width and on the overall value of  $\partial Q_{sc}$  can result in deviation from actual values, negative calculated values, and step functions for low temperature C-V calculated minority doping concentrations as seen in Figure 17.

## V. COMPENSATION IN ALTERNATE BIAS

### A. ALTERNATE BIAS OPERATION

Many of the fabrication issues crucial to extending wavelength response into the mid to far-IR are tied to the difficulty of growing highly pure, extremely thin blocking layers. When these conditions are not simultaneously achieved in the standard configuration (see Chapter I, Section C), performance is affected. In one limit an extremely thin, but impure blocking layer would not provide sufficient blocking of hopping current and would allow a high dark current. In another limit an ultimately pure blocking layer but with a graded transition region from heavily doped to highly pure would have the same results in a thin layer limit. Here the blocking layer needs to be grown thick enough to isolate the graded region from the active layer [11,12].

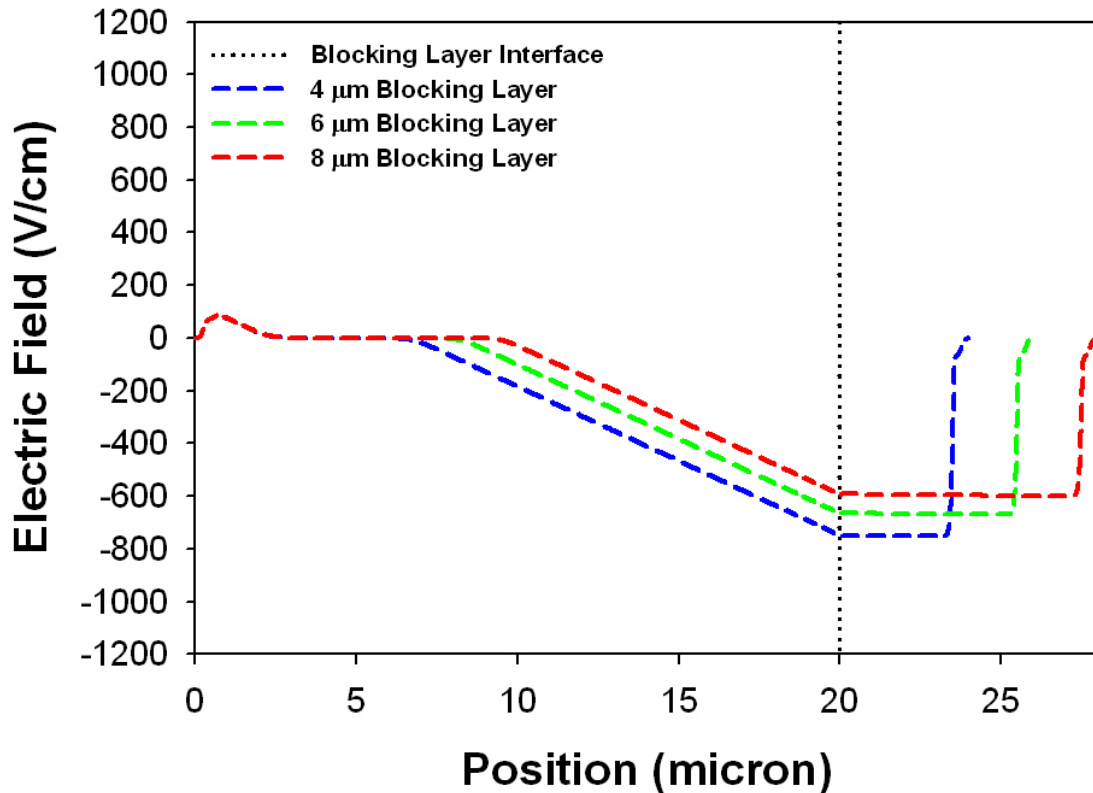


**Figure 22** Electric field as a function of position for several blocking layer thicknesses. Parameters the same as Table 1 except active layer minority doping  $5 \times 10^{12} \text{ cm}^{-3}$ , temperature 4.2 K, bias 0.75 V.

Growing thicker blocking layers is not a desirable solution in standard bias because, as shown in Figure 22, a thicker blocking layer results in significant loss in depletion width in the active layer and loss in charge collection and responsivity at a given bias. Keeping the blocking layer as thin as possible reduces both this loss of responsivity and the range of space charge effects identified through the earlier C-V analysis.

One proposed solution to these problems is to operate under an alternate bias [15]. In this configuration the bias is applied to the active layer contact rather than the blocking layer contact. With an n-type BIB this requires applying a positive bias to deplete into the compensated minority sites ( $N_A^-$ ) as seen in Figure 23. Here the photo-ionized donor sites will be pushed toward the blocking layer interface where the hopping current will be stopped, and the electrons in the conduction band will be collected at the active layer contact.

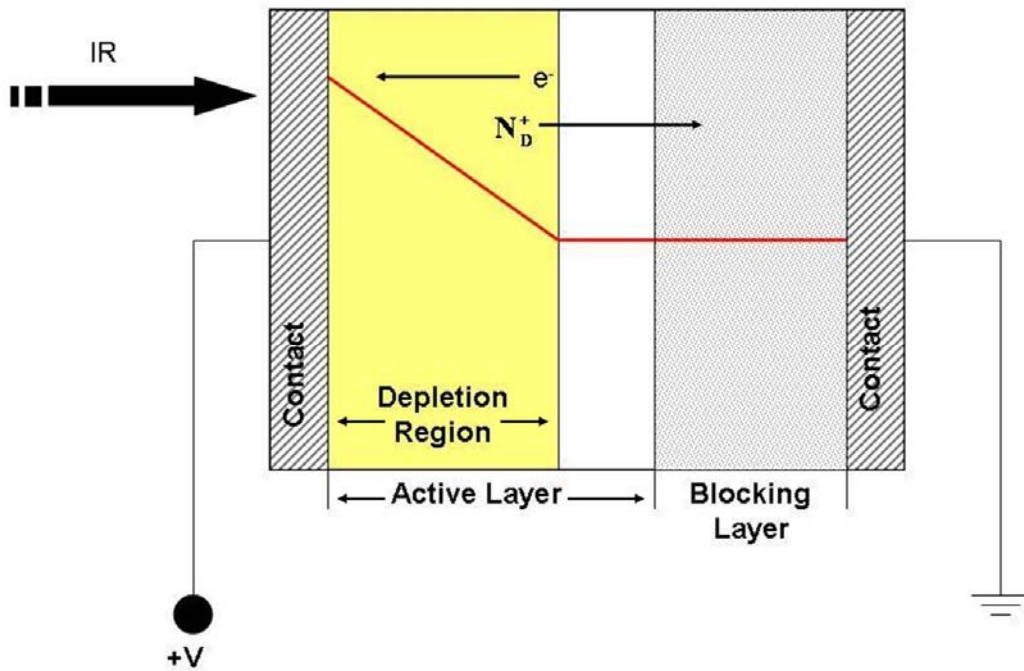


**Figure 23 Schematic diagram of alternate biased n-type BIB. Red line indicates the electric field distribution.**

For the alternate biased, p-type BIB in Figure 24 a negative bias must be applied to deplete into the positive compensated donor sites ( $N_D^+$ ). Here, the electric field will pull ionized holes in the valence band toward the active layer contact and push  $N_A^-$  carriers, the hopping current, toward the blocking layer where they will be stopped.

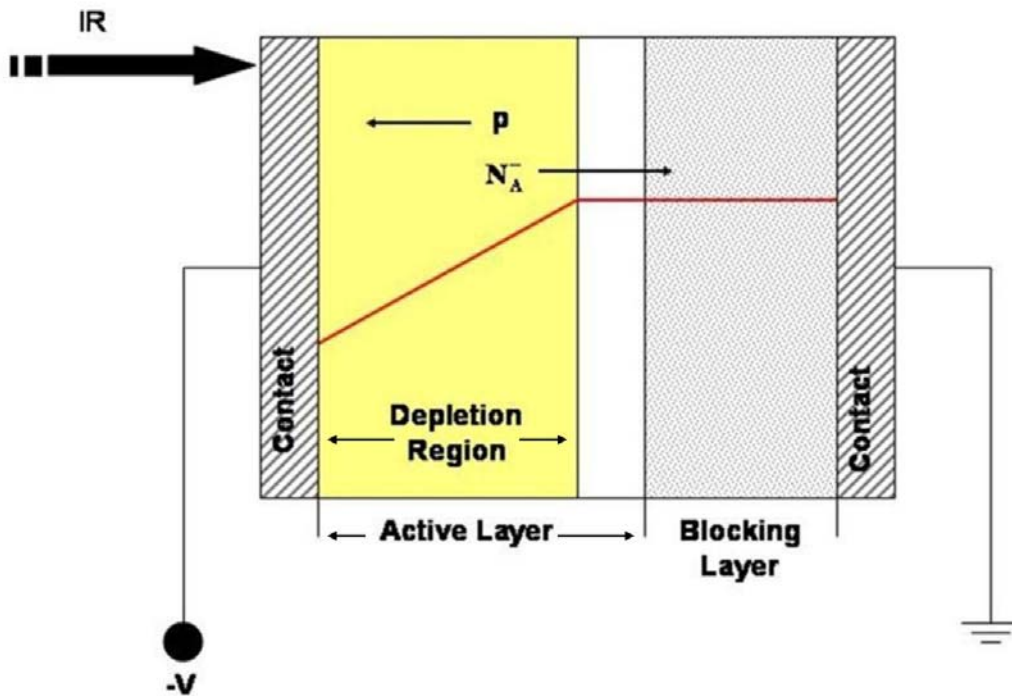


**Figure 24 Schematic diagram of alternate biased p-type BIB. Red line indicates the electric field distribution.**

This alternate bias configuration is desirable because it causes the electric field to deplete through the active layer first and results in a larger depletion region in the active layer as seen in Figure 25. This effect alone is desirable because it results in larger photocurrents in ideal blocking layer cases, although dark current may also be larger. The advantages become more pronounced when realistic blocking layer parameters for longer wavelength BIBs are taken

into account. The alternate bias allows for significantly thicker blocking layers while maintaining the depletion region in the active layer.

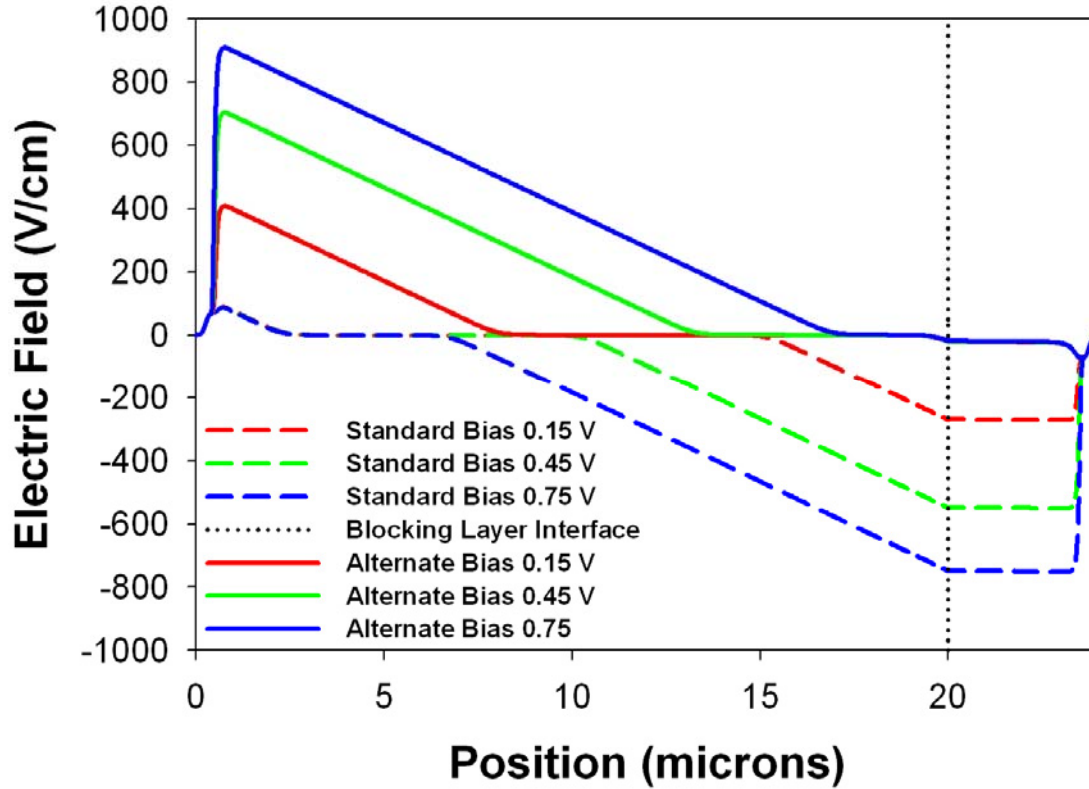


**Figure 25 Electric field as a function of position for standard and alternate biases. Parameters same as Table 1.**

The primary concern in this configuration is ensuring that the device does not saturate with dark current as a result of the alternate bias. The hopping current, which results from charge flow along the dopant band, is most critical and can be calculated in the model. Figure 26 shows the ionized donor current as a function of position for both standard and alternate bias. The purity of the blocking layer prevents the completion of the circuit which would allow the hopping current to flow continuously through the dopant band. In standard bias (n-type BIB) it is stopped because the highly pure blocking layer prevents the injection of ionized donors  $N_D^+$  from the blocking layer contact into the active layer. In alternate bias the same is true, only the ionized donors are being pushed toward the blocking layer and the high purity of the blocking layer, and



the associated low mobility for hopping conduction, prevents these carriers from reaching the contact.

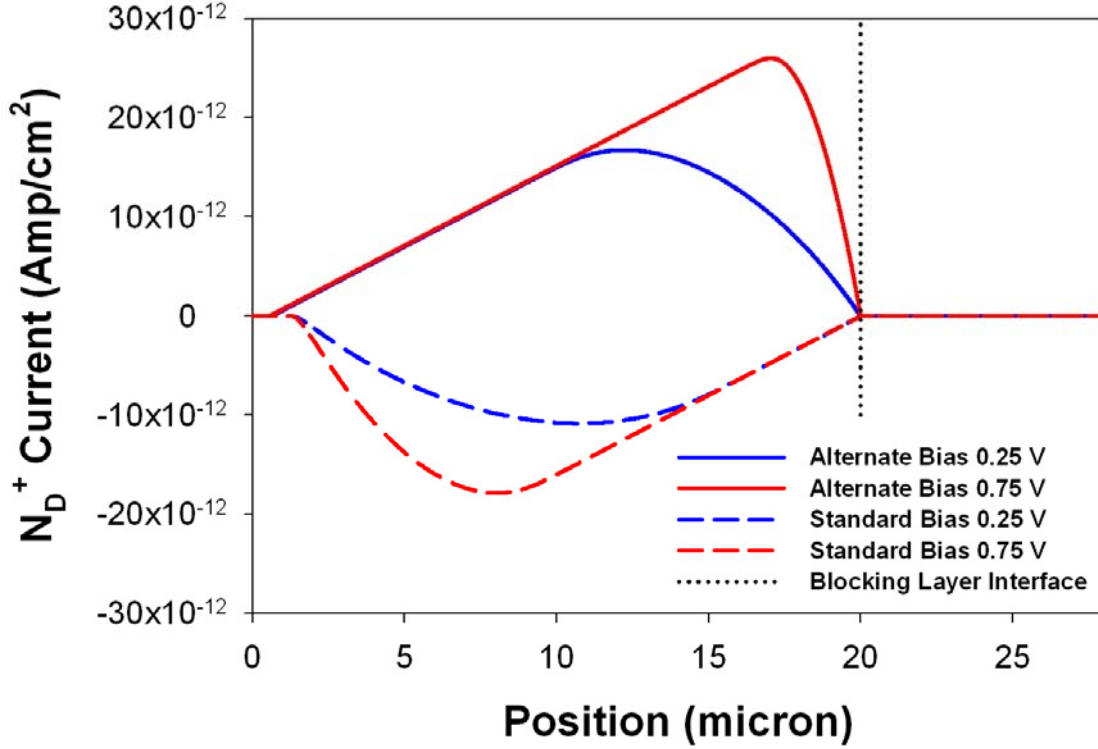


**Figure 26 Hopping current as a function of position for multiple biases and configurations. Parameters the same as Table 1 except active layer minority doping  $5 \times 10^{12} \text{ cm}^{-3}$ , temperature 4.2 K.**

Also of concern in alternate bias is the diffusion of charge carriers from the contacts. In standard bias, the carriers diffuse from both contacts and recombine, setting up near-contact space charge regions. The polarity of the applied field is such that in standard bias the charge carriers are pulled from the active layer contact into the active layer, and pushed from the blocking layer into the blocking layer contact on the other side as seen in Figure 27. The net result is that the significant Debye tail occurs in the heavily doped active layer. The extent of the Debye tail is determined by the trapping of free carriers by ionized sites and is therefore proportional to  $\sqrt{N_{\min}}^{-1/2}$ . In alternate bias, the injecting contact for free electrons is switched to the blocking layer as a result of the

switch in bias. Because the minority dopant concentration determines the rate of recombination and thus the length of the Debye tail, the purity of the blocking layer requires that it be thick enough to terminate the contact diffusion current prior to the active layer/blocking layer interface. Otherwise, the hopping current would have the necessary charge source and path to complete the circuit, raising the dark current to an unacceptable level.

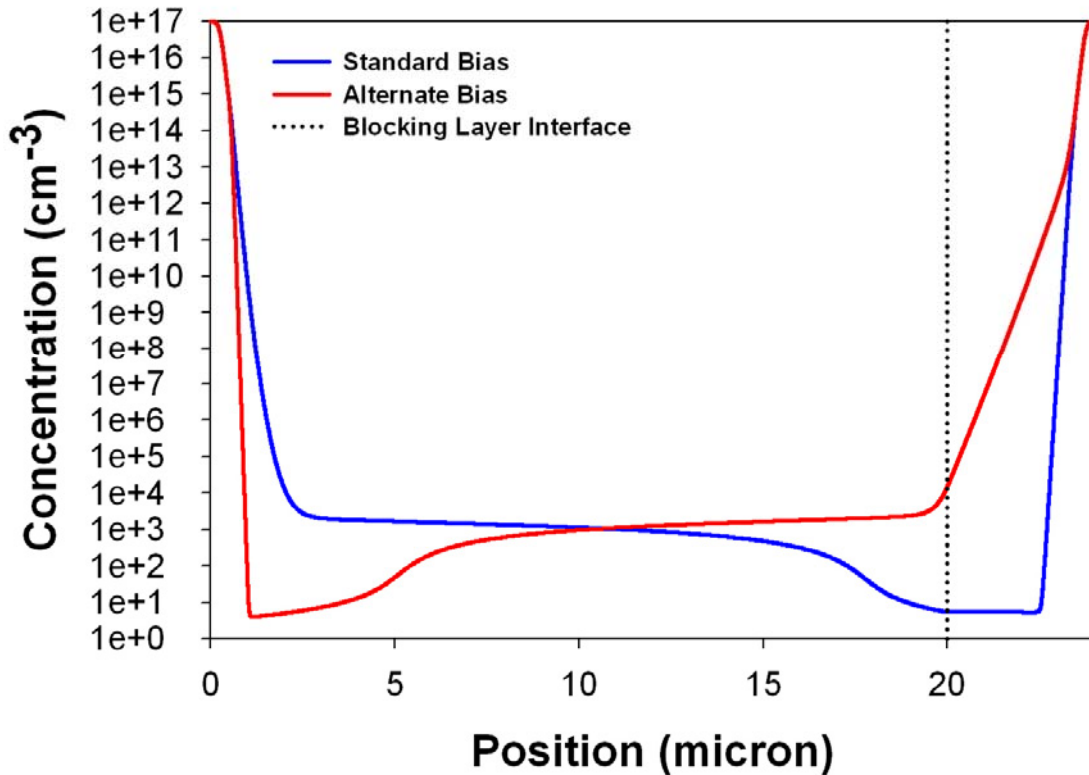


**Figure 27** Plot of free carrier concentration, showing Debye tails for standard and alternate bias. Parameters the same as Table 1 except active layer minority doping  $5 \times 10^{12} \text{ cm}^{-3}$ , temperature 4.2 K, bias 0.5 V.

## B. ALTERNATE CONFIGURATION IN GERMANIUM

The longer Debye tail and associated dark current in alternate bias could be a serious setback in the standard configuration. However, the strength of the alternate bias lies in its operational independence from blocking layer thickness. The potential impact of employing alternate bias for longer wavelength response

in Ge and GaAs is significant because it relaxes blocking layer thickness requirements. For the parameters shown in Table 2, Figure 28 demonstrates that devices in alternate bias have almost no decrease in depletion width for a blocking layer thickness of 50  $\mu\text{m}$ . When these thicknesses are modeled in the same devices in standard bias, Figure 28 shows the results are very small depletion widths in the active layer and a resulting small photocurrent.

Absorbing Layer Majority Doping	$1.0 \times 10^{16} \text{ cm}^{-3}$
Absorbing Layer Minority Doping	$4.0 \times 10^{12} \text{ cm}^{-3}$
Absorbing Layer Thickness	30 $\mu\text{m}$
Blocking Layer Majority Doping	$2.0 \times 10^{12} \text{ cm}^{-3}$
Blocking Layer Minority Doping	$1.0 \times 10^{11} \text{ cm}^{-3}$
Blocking Layer Thickness	50 $\mu\text{m}$
Temperature	2.5 K
Bohr Radius	$37 \times 10^{-8} \text{ m}$
Interface Grade Parameter	$2.0 \times 10^{-7} \text{ cm}$
Contact Grade Parameter	$1.0 \times 10^{-5} \text{ cm}$
Optical Flux Rate $\gamma$	$1.0 \times 10^{-9} \text{ s}^{-1}$ for Photo-Current

**Table 2 Ge BIB parameters**

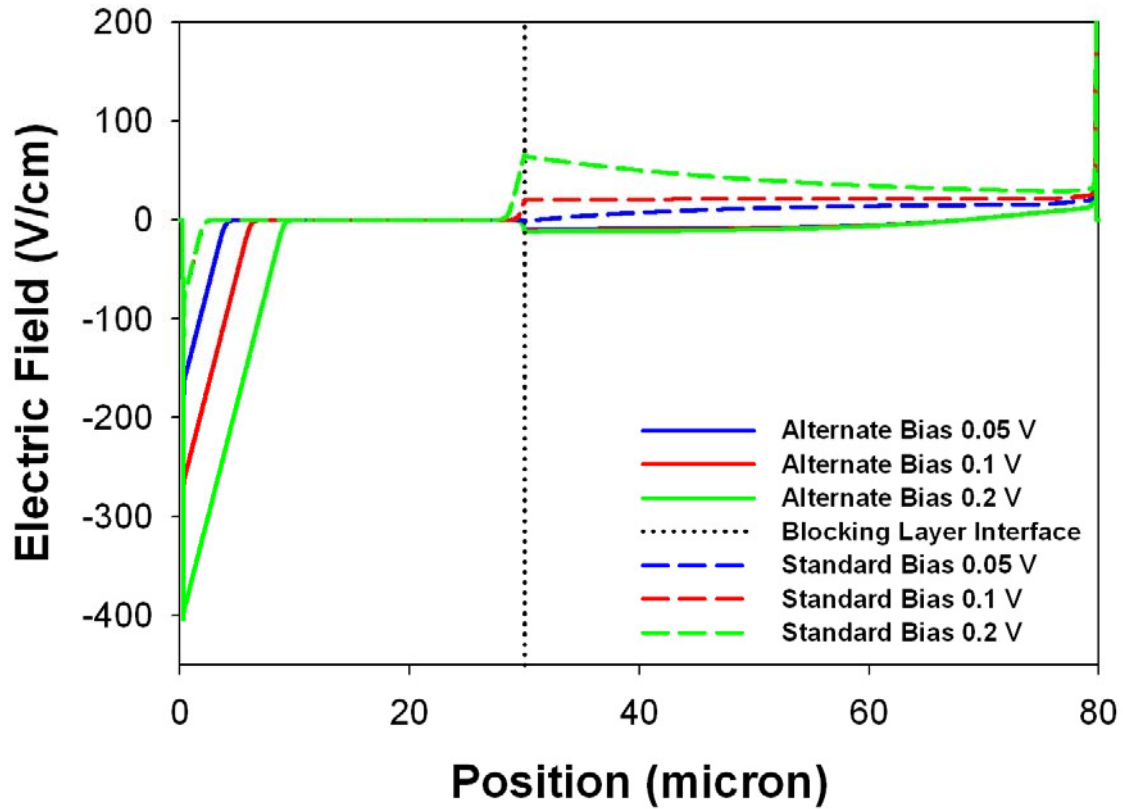


**Figure 28 Electric field as a function of position for standard and alternate bias in Ge. Parameters listed in Table 2.**

However, the success of this approach is highly dependent upon the minority doping level in the blocking layer. When the same Ge device is modeled in alternate bias with a higher minority doping level, the voltage drop occurs almost exclusively in the blocking layer. The increase in resistivity of the blocking layer causes an increase in voltage drop that becomes significant for the large thickness. Figure 29 illustrates this field distribution, and shows that devices require minority dopant concentrations at around or below  $1 \times 10^{11} \text{ cm}^{-3}$  to deplete adequately into the active layer.

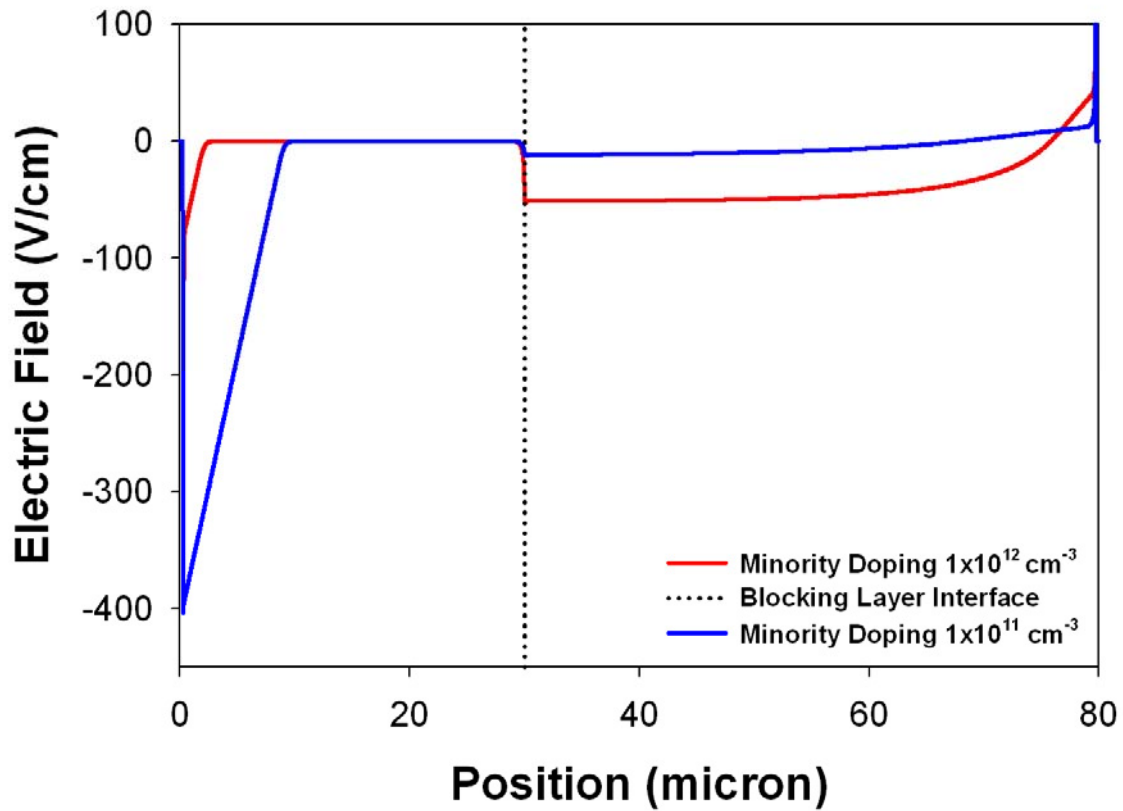


**Figure 29 Electric Field as a function of doping, Ge. Parameters listed in Table 2, varied minority doping, alternate biased 0.2 V.**

Once again minority doping concentrations, in this case in the blocking layer, are crucial to the success or failure of any attempts to build the devices. The alternate bias configuration offers a significant relaxation of blocking layer growth requirements with performance improvements, assuming these doping levels can be held to a low enough level in a reasonable growth thickness ( $\sim 50 \mu\text{m}$ ).

THIS PAGE INTENTIONALLY LEFT BLANK

## VI. CONCLUSIONS

### A. SUMMARY

Current attempts to extend BIB response into the 40-350  $\mu\text{m}$  range using Ge or GaAs have been slowed by fabrication difficulties. Despite this, the potential of these materials for large arrays and for new applications in the terahertz regime continue to drive the industry to arrive at solutions. The application of alternate bias configuration for Ge devices shows that blocking layer thicknesses can be increased significantly, thereby alleviating one of the key constraints on realizing a far-infrared Ge BIB. The minority doping concentration remains crucial and the alternate bias will only work if these levels are kept low enough. In this work, it has been established that the minority doping levels in the blocking layer must be kept at or below  $1 \times 10^{11} \text{ cm}^{-3}$  for Ge BIBs. GaAs devices likewise rely upon low compensation levels, although for this material the difficulties arise in the active layer rather than the blocking layer. The end result is that performance of BIBs using either of these materials requires control of compensation levels in both the active and blocking layers of these devices. Problems with accurately measuring the minority doping concentration exacerbate the already difficult situation.

The numerical model's ability to solve for space charge throughout BIB devices made it ideal for analyzing the low temperature C-V profiling method of determining minority doping. Using this, we have demonstrated the important role of space charge in the blocking layer in the application of C-V profiling for measuring minority doping concentration, particularly for the case of graded interfaces in BIB devices. Modeled results closely resemble experimentally achieved results and explain the presence of step functions and overall variation from expected values.

## **B. FUTURE WORK**

This thesis provides a basic explanation of unexpected minority doping variations in low temperature C-V measurements. The next step needs to be determination of the actual grade between the active layer and the blocking layer for the experimental results presented (Figure 13). Spreading resistance data can be obtained, and this will test our assertion that the unexpected data is a result of the grade between the active and blocking layers.

This thesis has highlighted ramifications of the limiting assumption of a space charge free blocking layer, however the question of correcting this problem has not been addressed. A thorough investigation of this space charge needs to be conducted to isolate exactly what effects it has upon calculations. A full understanding of these characteristics should make it possible to modify the assumptions and solve for the actual minority doping concentration.

Finally, fabrication of a BIB device specifically for testing and validation of the alternate bias configuration is crucial for acceptance by industry. The potential for far-infrared response, particularly for Ge BIBs, must be explored in the laboratory with thicker blocking layers to test the results achieved in simulations at the Naval Postgraduate School.



## LIST OF REFERENCES

- 1 Petroff M. D. and M. G. Stapelbroek, US Patent No 4568960 (4 February 1986).
- 2 Huffman J. E., A. G. Crouse, B. L. Halleck, T. V. Downs, and T. L. Herter, Journal of Applied Physics **72**, 273 (1992).
- 3 Haegel N. M., Nuclear Instruments and Methods in Physics Research, **377**, 503 (1996).
- 4 Hogue H. H., M. T. Guptill, D. B. Reynolds, E. W. Atkins, and M. G. Stapelbroek, Proceedings SPIE **4850**, 880 (2003).
- 5 Ennico K., M. McKelvey, C. McCreight, R. McMurray, Jr., R. Johnson, A. W. Hoffman, P. Love, and N. Lum, Proceedings SPIE **4850**, 890 (2003).
- 6 Szmulowicz F. and F. L. Madarsz, Journal of Applied Physics **62**, 2534 (1987).
- 7 Reike G. H., *Detection of Light: From the Ultraviolet to the Submillimeter*. (Cambridge University Press, Cambridge, 2003), pp. 68-74.
- 8 Haegel N. M., J. E. Jacobs, and A. M. White, Applied Physics Letters **77**, 4389 (2000).
- 9 Haegel N. M., S. A. Samperi, and A. M. White, Journal of Applied Physics **93**, 1305 (January 2003).
- 10 White A. M., "Numerical Analysis of Extrinsic Detectors," Personal Correspondence (January 2004).
- 11 Reichertz L. A., J. W. Beeman, B. L. Cardozo, N. M. Haegel, E. E. Haller, G. Jakob, and R. Katterloher, Proceedings SPIE **5543**, 231 (2004).
- 12 Bandaru J., J. W. Beeman, E. E. Haller, S. Samperi, and N. M. Haegel, Infrared Physics and Technology **43**, 357 (2002).
- 13 Sze S. M., *Physics of Semiconductor Devices* (John Wiley & Sons, Inc., New York, 1981), pp. 248-249.
- 14 Love P., "NPS Visit", Personal Correspondence (2 June 2004).
- 15 Garcia J. C., N. M. Haegel, and E. A. Zagorski, Applied Physics Letters **87**, 043502 (2005).

THIS PAGE INTENTIONALLY LEFT BLANK

## INITIAL DISTRIBUTION LIST

1. Defense Technical Information Center  
Ft. Belvoir, Virginia
2. Dudley Knox Library  
Naval Postgraduate School  
Monterey, California
3. Professor Nancy M. Haegel  
Naval Postgraduate School  
Monterey, California
4. Professor Don Walters  
Naval Postgraduate School  
Monterey, California
5. Professor James H. Luscombe  
Naval Postgraduate School  
Monterey, California
6. Dr. Peter Love  
Raytheon Vision Systems  
Goleta, California
7. Dr. Craig McCreight  
NASA AMES  
Moffett Field, California
8. Professor Eugene Haller  
University of California, Berkeley  
Berkeley, California
9. Lothar Reichertz  
University of California, Berkeley  
Berkeley, California
10. Jeff Beeman  
University of California, Berkeley  
Berkeley, California